JOURNAL OF ABDOMINAL WALL SURGERY
EUROPEAN HERNIA SOCIETY

TYPE Review
PUBLISHED 25 November 2026
DOI 10.3389/jaws.2026.17879

Check for updates

OPEN ACCESS

*CORRESPONDENCE
Francesco Brucchi,
francesco.brucchi@unimi.it

RECEIVED 19 September 2026
REVISED 15 November 2026
ACCEPTED 17 November 2026
PUBLISHED 25 November 2026

CITATION
Brucchi F, Sassun R, Cirocchi R and Dionigi G (2026) Quantitative functional imaging of abdominal wall biomechanics: a scoping review of imaging modalities, candidate biomechanical biomarkers, and clinical applications.
J. Abdom. Wall Surg. 5:17879.
doi: 10.3389/jaws.2026.17879

COPYRIGHT
© 2026 Brucchi, Sassun, Cirocchi and Dionigi. This is an open-access article distributed under the terms of the Creative Commons Attribution License (CC BY). The use, distribution or reproduction in other forums is permitted, provided the original author(s) and the copyright owner(s) are credited and that the original publication in this journal is cited, in accordance with accepted academic practice. No use, distribution or reproduction is permitted which does not comply with these terms.

Quantitative functional imaging of abdominal wall biomechanics: a scoping review of imaging modalities, candidate biomechanical biomarkers, and clinical applications

Francesco Brucchi[1,2]*, Richard Sassun[3], Roberto Cirocchi[4] and Gianlorenzo Dionigi[1,2]

[1]Department of Pathophysiology and Transplantation, University of Milan, Milan, Italy, [2]Division of General Surgery, Istituto Auxologico Italiano, IRCCS (Istituto di Ricovero e Cura a Carattere Scientifico), Milan, Italy, [3]General Surgery Unit, Pio XI Hospital, Desio, Monza e Brianza, Italy, [4]Department of Medicine and Surgery, University of Perugia, Perugia, Italy

Background: Ventral and incisional hernia repair remains burdened by recurrence, bulging, and impaired trunk function, and key operative decisions (e.g., component separation or transversus abdominis release [TAR], preoperative botulinum toxin A [BTA], mesh choice) are still made largely without objective measures of how the wall behaves under load. Conventional imaging is predominantly anatomical, whereas the abdominal wall is a dynamic, load-bearing structure. Because the literature on quantitative functional imaging is fragmented across surgery, radiology, and biomechanics, we mapped it to answer three questions: (1) which *in vivo* imaging modalities have been used to quantify abdominal wall mechanical function; (2) which candidate biomarkers they generate, under which loading conditions, and with which measurement properties; and (3) how these measurements have been linked to clinical applications.

Methods: This scoping review followed the Arksey–O'Malley framework, JBI guidance, and PRISMA-ScR. PubMed/MEDLINE, Embase, and Web of Science were searched for *in vivo* imaging studies reporting quantitative measures of abdominal wall mechanical function. Diagnostic-only imaging, adhesion or mesh visualization, and qualitative mobility assessment were excluded. Studies were charted by population, modality, loading state, structure, candidate biomarker, measurement properties, and clinical linkage.

Results: The searches identified 1,992 records; after removal of 164 cross-database duplicates, 1,827 were screened, 52 reports were assessed in full text, and 45 were included, several from linked research programs with potentially overlapping cohorts. Twenty-two used SWE/ARFI, four dynamic MRI, six functional/stress CT, six dynamic ultrasound/M-mode, and seven optical, photogrammetric, or indentation-based methods. Protocols, loading tasks, structures, and units were highly heterogeneous. Elastographic stiffness values depended on loading state, imaging plane, probe pressure, and layer geometry, and registration-derived strain on algorithmic assumptions.

Conclusion: Quantitative functional imaging can characterize abdominal wall stiffness, deformation, displacement, contractility, compliance, and stress-dependent geometry *in vivo*, but the evidence remains exploratory and does

not support routine imaging-guided reconstruction. Reported values are load- and protocol-dependent and should not be interpreted as intrinsic material constants. Standardized acquisition, measurement-error thresholds, reference ranges, and prospective validation against surgical decisions, patient-reported function, and recurrence, together with assessment of incremental value over established patient- and surgeon-related predictors, are required before clinical implementation.

KEYWORDS

abdominal wall, biomechanics, dynamic MRI, functional CT, functional imaging

Introduction

The abdominal wall is not a static envelope. It is a multilayered musculo-aponeurotic system that continuously changes shape and tension during breathing, coughing, Valsalva, trunk movement, and variations in intra-abdominal pressure. Yet most preoperative imaging used in abdominal wall surgery remains primarily anatomical: defect width and location, loss of domain, muscle morphology, rectus separation, and mesh or scar-related findings are typically assessed on static cross-sectional images. This creates a mismatch between the dynamic biological system that surgeons reconstruct and the predominantly static measurements used to characterize it.

A growing body of work has therefore attempted to measure abdominal wall mechanics *in vivo*. Ultrasound shear-wave elastography and ARFI provide estimates of tissue stiffness or shear-wave propagation [1–22]. Dynamic MRI can track muscle geometry, regional displacement, and deformation during physiological maneuvers [23–25] and, when combined with simultaneous independent measurement of intra-abdominal pressure, can characterize pressure–motion relationships [26]. Functional or stress CT can compare rest with active contraction or Valsalva and quantify contractility, bulging, displacement, strain, or stress-dependent geometry [27–32]. Dynamic ultrasound and M-mode methods can quantify contraction-related thickness change, tissue deformation, and deformation timing [33–38]. Optical and surface-mechanics approaches provide complementary pressure- or load-coupled measurements of wall deformation and material behavior [39–45].

Abbreviations: ARFI, acoustic radiation force impulse; BTA, botulinum toxin A; CT, computed tomography; DIEAP, deep inferior epigastric artery perforator (flap); DIR, deformable image registration; DRA, diastasis recti abdominis; eTEP, enhanced-view totally extraperitoneal (repair); EO / IO / TrA, external oblique / internal oblique / transversus abdominis; IAP, intra-abdominal pressure; IH / VH, incisional hernia / ventral hernia; IRD, inter-rectus distance; LOD, loss of domain; MRI, magnetic resonance imaging; NMES, neuromuscular electrical stimulation; PCC, Population–Concept–Context (eligibility framework); PRISMA-ScR, Preferred Reporting Items for Systematic reviews and Meta-Analyses extension for Scoping Reviews; PROMs, patient-reported outcome measures; RA, rectus abdominis; sEMG, surface electromyography; SWE, shear-wave elastography; SWS / SWV, shear-wave speed / shear-wave velocity; TAR, transversus abdominis release; TDI, tissue deformation index (M-mode sonography); ms-TRAM, muscle-sparing transverse rectus abdominis myocutaneous (flap); W3, European Hernia Society transverse width grade W3 (≥10 cm).

Biomechanical background: the stress–strain relationship

All measurements mapped in this review can be located on one basic relation, the stress–strain curve (Figure 1; Glossary). Stress (σ) is force per unit cross-sectional area; strain (ε) is the change in length relative to the original length. For the intact wall, the corresponding structural quantities are load (intra-abdominal pressure, or membrane tension per unit width) and deformation (displacement or elongation). The slope of the curve is stiffness: a modulus (kPa) for a material, force per unit displacement (N/mm) for a structure; its inverse is compliance. For metals within their working range this slope is constant, so that one coefficient, Young's modulus, is sufficient. Collagenous soft tissues such as the linea alba, the rectus sheath, and the aponeuroses behave differently: their curve is J-shaped [46, 47]. At low load, crimped collagen fibers straighten and re-orient, and large strain is produced by little stress (the "toe" region). As fibers are progressively recruited the curve steepens (the "heel") and then enters an approximately linear region of high stiffness, which ends in yield and failure. Stiffness is therefore not a single number: it depends on where on the curve the tissue is operating, and what can be measured at a given state is the local slope (tangent modulus). *In vivo* the wall is never at the origin of this curve. Intra-abdominal pressure and muscle tone impose a prestress that sets the operating point, and Valsalva, coughing, or contraction move it up the curve; active muscle contraction additionally changes the curve itself, a contribution that is under neural control and absent in excised tissue. The relation also differs with direction (anisotropy; the linea alba, for example, is more compliant longitudinally than transversely [47]) and with time: loading and unloading paths do not coincide (hysteresis), tissue creeps under sustained load and relaxes under sustained deformation (viscoelasticity), and the response changes over repeated load cycles (preconditioning and, at higher loads, permanent deformation and fatigue).

Stress measure and reference state

The definitions given above are unambiguous only for small deformations. For the large deformations of the abdominal wall, the value stated for a stress or a strain depends on the configuration to which force and length are referred. Cauchy (true) stress is force per unit of current, deformed area. The first Piola–Kirchhoff (nominal) stress is force per unit of area in the reference configuration. The second Piola–Kirchhoff stress is defined entirely in the reference

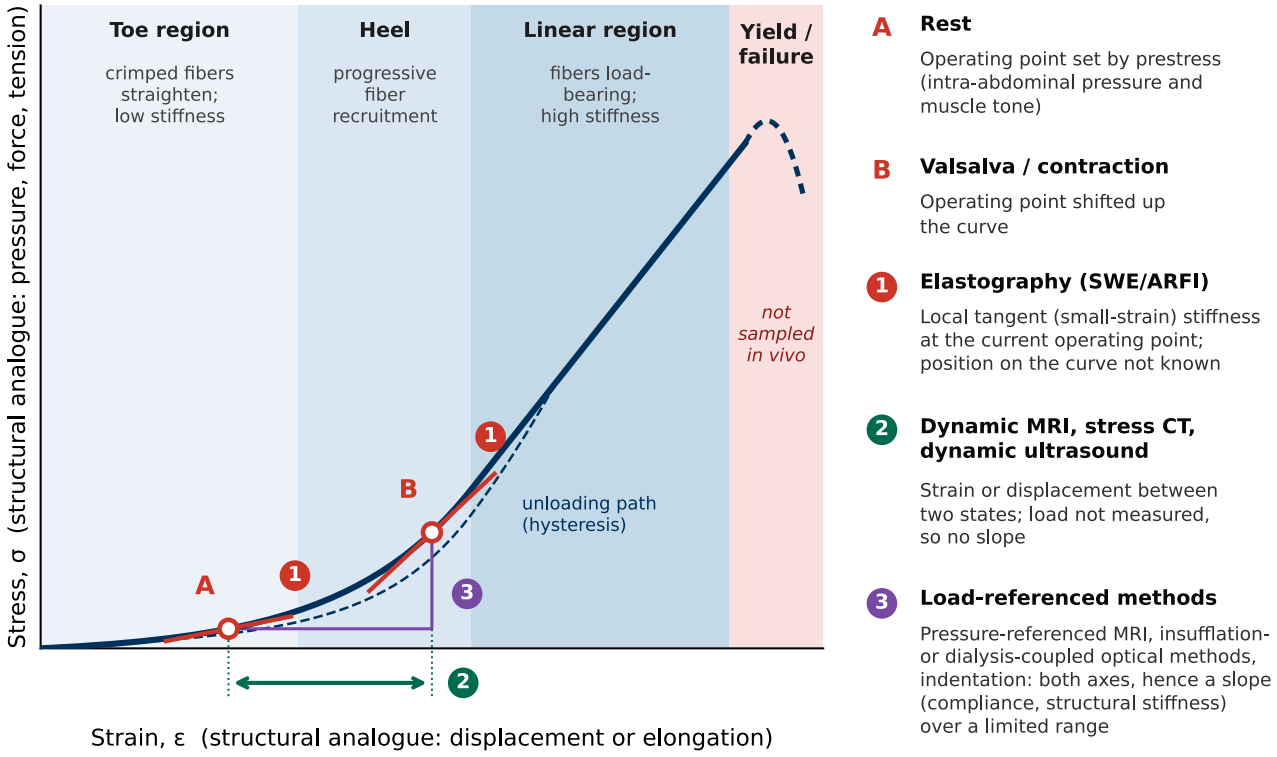


FIGURE 1
Schematic stress–strain relationship of collagenous abdominal wall tissue and the part of it sampled by each imaging family. The curve is J-shaped: a compliant toe region, in which crimped collagen fibers straighten; a heel, in which fibers are progressively recruited; an approximately linear region of high stiffness; and yield and failure. *In vivo*, intra-abdominal pressure and muscle tone set the operating point at rest **(A)**; Valsalva or contraction moves it up the curve **(B)**. (1) Elastography returns the local tangent stiffness at the current operating point, whose position on the curve is not known. (2) Dynamic MRI, stress CT, and dynamic ultrasound measure strain or displacement between two states without the corresponding load. (3) Load-referenced methods measure both axes, and therefore a slope, over a limited range. Stress denotes Cauchy (true) stress; *in vivo*, deformation is measured from the resting state A and not from the unloaded origin of the curve. The dashed line indicates the unloading path (hysteresis). The failure region is not sampled *in vivo*. The curve is schematic, is not drawn to scale, and does not represent measured data; the additional effect of active muscle contraction on the shape of the curve is not shown. ARFI, acoustic radiation force impulse; CT, computed tomography; MRI, magnetic resonance imaging; SWE, shear-wave elastography.

configuration; it is the work-conjugate of the Green–Lagrange strain and the usual output of hyperelastic constitutive models [46, 48]. Throughout this review, "stress" denotes Cauchy stress, and deformation is referred to the resting abdomen. We prefer this convention for three reasons. First, the stress-free configuration of the abdominal wall cannot be observed *in vivo*: the wall at rest is already loaded by intra-abdominal pressure and muscle tone, so that the resting state is the only reference configuration available to imaging. Second, Cauchy stress is the stress that balances intra-abdominal pressure in the current geometry (for a thin wall it follows from pressure, current curvature, and current thickness by Laplace's law) and can therefore be estimated without knowledge of the stress-free state. Third, it is the stress actually carried by tissue, suture line, and mesh, and hence the quantity relevant to failure. Two consequences follow. Strains measured from the resting state are incremental: they omit the unknown deformation between the stress-free and the resting configuration, so that a point measured *in vivo* cannot be placed on an *ex-vivo* curve, which starts from the unloaded state, without an assumption about prestress. And a slope obtained from such strains is a tangent stiffness at the resting operating point, not a modulus of the unloaded tissue.

Effect of using other measures

The choice of measure matters increasingly as deformation grows. For a uniaxial stretch λ (deformed length divided by reference length) of an incompressible material, Cauchy stress equals λ times the first and λ^2 times the second Piola–Kirchhoff stress; the same stretch corresponds to an engineering strain of $\lambda - 1$, a Green–Lagrange strain of $(\lambda^2 - 1)/2$, and a logarithmic strain of $\ln \lambda$. At a stretch of 1.2, i.e., an elongation of 20%, Cauchy stress therefore exceeds the first Piola–Kirchhoff stress by 20% and the second by 44%, and the three strain measures are 0.20, 0.22, and 0.18. A secant modulus computed from Cauchy stress and logarithmic strain is then about 1.7 times the one computed from second Piola–Kirchhoff stress and Green–Lagrange strain, although both describe the same experiment on the same material. The measures converge at small strains and can be converted into one another when the deformation gradient is known, so that none of them is wrong; but values are comparable between studies only if the stress measure, the strain measure, and the reference configuration are stated. Among the included reports these were not reported uniformly: strain appears, for example, as the percentage change of a linear

TABLE 1 Landscape of quantitative candidate biomarkers by imaging family, mapped to loading states, populations, and clinical linkage.

Imaging family (n)	Representative candidate biomarkers (units)	Loading/activation states used	Populations studied	Highest clinical linkage reached/ key gap
Ultrasound SWE/ARFI (n = 22)	Measured: Shear-wave speed, c (m/s). Derived: shear modulus, $\mu = \rho c^2$ (kPa); Young's modulus, $E \approx 3\mu$ (kPa), reported as "stiffness" or "elasticity" in some studies. Other: SWV-to-thickness ratio; texture features Stress–strain relation: local small-strain tangent stiffness at the prevailing operating point; neither stress nor strain is measured, and the position on the curve is unknown	Rest; quiet and forced breathing; Valsalva; active abdominal inflation; isolated NMES contraction; pullback loading	Healthy volunteers; incisional hernia; pregnancy/postpartum DRA; obesity; multiparous women; W3 hernia with BTA; pediatric closure; lipoabdominoplasty	Reliability and graded-loading studies; longitudinal pregnancy/postpartum and postoperative change; disease-, width-, age-, and body-habitus associations. Added plane- and probe-pressure reliability evidence. Gap: operator/ anisotropy/layer/depth bias; no loading-validated clinical thresholds
Dynamic MRI (n = 4)	Circumferential/radial strain (%); muscle length and thickness change; regional displacement (mm); pseudo-compliance; pressure–motion coupling Stress–strain relation: Strain/ displacement axis only; a slope (pseudo-compliance) is obtained only when intra-abdominal pressure is measured simultaneously [26]	Controlled and forced breathing; coughing; Valsalva; ± synchronized intra-abdominal pressure	Healthy volunteers; ventral hernia pre/post repair	Feasibility of longitudinal pre/ post-repair phenotyping (n = 11). Gap: Small cohorts; demanding post-processing; not routine; DIR-derived layer strain sensitive to sliding fascial interfaces; pressure–motion coupling requires independent IAP measurement
Functional/stress CT (n = 6)	Segmental contractility/paralysis grade; muscle elongation; stress-induced bulging; contour eccentricity; rectus width/area; semilunar-line distance Stress–strain relation: Strain/ displacement axis between two states (rest versus crunch or Valsalva); load is not measured, so that "elasticity" is a relative, two-point estimate	Rest vs. active 'crunch' contraction; Valsalva stress vs. non-stressed acquisition; pre/ post-op	Complex ventral/incisional hernia; diastasis recti; BTA-treated cohorts; post-eTEP	Embedded in complex-hernia pathways; patient-specific elasticity, BTA effects, postoperative contour, GRIP/ CRIP planning, and HEDI displacement/strain mapping. Gap: radiation; no standard functional-CT definition; linked/overlapping cohorts. DIR-derived strain sensitive to sliding fascial interfaces
Dynamic ultrasound/ M-mode myosonography (n = 6)	Rectus thickness at rest/contracted; contraction-related thickness change; tissue deformation index (TDI, %/ms); connective-tissue deformation; deformation onset; strain rate Stress–strain relation: strain axis (thickness change) and its rate during active contraction; reflects activation rather than the passive tissue response; load is not measured	Relaxed vs. maximal voluntary contraction; rapid loaded arm abduction; longitudinal pre/ postoperative assessment	Healthy volunteers; abdominal-flap breast reconstruction/DIEP donor site	Reliability and normative TDI characterization; serial donor-site functional assessment. Gap: heterogeneous tasks; limited surgical validation

(*Continued*)

TABLE 1 Continued

Imaging family (n)	Representative candidate biomarkers (units)	Loading/activation states used	Populations studied	Highest clinical linkage reached/ key gap
Optical/photogrammetric/ indentation surface mechanics (n = 7)	Pressure-volume displacement/ compliance; 3D displacement; strain; stress; Young's modulus; principal strain fields/directions; force–displacement structural stiffness (N/mm); hyperelastic Ogden parameters Stress–strain relation: both axes (pressure or force versus displacement or strain); slope (compliance, structural stiffness) and, with a model, constitutive parameters over the tested load range; whole wall rather than single layer	Passive expiration; CO2 insufflation; contraction; peritoneal-dialysis filling; local indentation with relaxed/ activated muscles	Healthy volunteers; tetraplegia; laparoscopic patients; peritoneal-dialysis patients	Direct load-deformation coupling, anisotropy, regional clustering, and inverse-FEA material identification. Gap: Small cohorts; specialized setups; heterogeneous loading environments

Counts refer to the current 45-report synthesis. "Clinical linkage" denotes the most advanced link to a surgical decision or patient outcome reached within each family; it should not be interpreted as evidence of validated clinical utility. The entry "Stress–strain relation" indicates which part of the basic stress–strain relationship (Figure 1) each imaging family samples. Units: m/s denotes directly measured shear-wave speed; kPa denotes model-derived shear modulus ($\mu = \rho c^2$) or Young's modulus ($E \approx 3\mu$), which are not interchangeable; N/mm denotes structural force–displacement stiffness of the whole wall. Potentially non-independent (linked) reports, whose participant numbers should not be summed: SWE/ARFI [3, 4, 6]; dynamic MRI [23–26]; functional/stress CT [27, 28] and [30–32]; dynamic ultrasound/M-mode [35, 36]; surface mechanics [41, 45]. DIR, deformable image registration; IAP, intra-abdominal pressure.

dimension, as principal strain, or as Green–Lagrange strain [32, 41], and the reference state as rest, a breathing phase, or the abdomen before insufflation or fluid filling. Shear-wave elastography is least affected by the choice of tensor, because the superimposed perturbation is very small; its difficulty is the dependence of wave speed on prestress (acoustoelastic effect), which is a property of the tissue state and not of the stress definition. We therefore recommend that studies reporting stress, strain, or a modulus of the abdominal wall name all three: the stress measure, the strain measure, and the reference configuration.

Each imaging family samples this relation differently and incompletely (Figure 1). Elastography superimposes a very small shear perturbation on the tissue at its current operating point: it returns a local, small-strain tangent stiffness at a position on the curve that is not known, which is why values rise with Valsalva or contraction. Dynamic MRI, stress CT, and dynamic ultrasound report the strain or displacement axis only, usually between two states such as rest and Valsalva; without simultaneous measurement of the load, no slope can be derived. Only load-referenced methods (pressure-referenced MRI, insufflation- or dialysis-coupled optical methods, and indentation) provide both axes and can therefore estimate a slope (compliance or structural stiffness) or the parameters of a constitutive model, and then only over a limited part of the curve and usually for the whole multilayer wall rather than for a single tissue. No *in vivo* modality samples the failure region, and time-dependent and cyclic behavior has hardly been addressed (Section *Discussion*). Tables 1–3 indicate, for each family and each candidate application, which part of this relation is sampled; the corresponding entry for each of the 45 included reports is given in Supplementary Table S3.

Terminology: measured quantity, mechanical parameter, and biomarker

"Biomarker" is not a term of mechanics. In engineering, the design of a load-bearing structure rests on coefficients and relations (moduli, compliance, strength, fatigue limits) obtained from standardized static and cyclic testing. A biomarker, in contrast, is a characteristic of the patient that is measured because it indicates normal biology, disease, or the response to an exposure or intervention [51]. To relate the two vocabularies, we distinguish three levels. (i) A measured quantity is what the device records: shear-wave speed, displacement, thickness, pressure, or force. (ii) A mechanical parameter is a coefficient or relation derived from measured quantities through a stated model and referred to the stress–strain relation: strain, modulus, structural stiffness, or compliance. (iii) A biomarker is a quantity of either kind that, obtained under a specified loading state, has been shown to be reliable and to carry diagnostic, prognostic, predictive, or monitoring information about the patient. A mechanical parameter becomes a biomarker only through such clinical qualification; conversely, a quantity need not be an intrinsic material constant to serve as a biomarker, provided that the loading conditions under which it is obtained are fixed and reported. All imaging outputs identified in this review are level (i) or level (ii) quantities, and none has completed clinical qualification. They are therefore referred to throughout the manuscript as candidate biomarkers.

These techniques have potential clinical relevance because, if shown to be reproducible and outcome-linked, imaging-derived measures of stiffness, deformation, contractility, or compliance might distinguish mechanical phenotypes that appear similar on static imaging, quantify responses to interventions such as BTA, and

TABLE 2 Cross-cutting measurement properties and principal sources of uncertainty.

Domain	Evidence signal	Representative studies	Implication
Repeatability/reliability	Acceptable for selected SWE and M-mode measures, but variable by muscle depth and protocol	[2, 7, 11, 35, 36]	Report ICC/SEM/MDC and acquisition success for each structure; do not generalize reliability across muscles
Probe pressure	Freehand compression can alter thickness and shear modulus	[22]	Control or document probe force, particularly for serial or between-group comparisons
Imaging plane/anisotropy	Shear-wave values and image stability depend on transducer orientation and fiber direction	[21]	Standardize imaging plane and report fiber alignment
Layer/depth effects	Layered wave propagation and deep-muscle acquisition can bias or reduce measurement reliability	[5, 11]	Report depth, layer, ROI dimensions, and device settings; avoid universal cut-offs
Prestress/nonlinearity	Shear-wave speed rises with tensile prestress from intra-abdominal pressure and activation; thin layers support guided (dispersive) waves	[1, 5, 7, 26]	Report shear-wave speed (m/s) with loading state; do not interpret derived moduli as intrinsic, load-independent constants
Image registration/sliding interfaces	Smoothness-regularized DIR across sliding fascial planes suppresses interlayer slip and may create artifactual intramuscular strain	[23–26, 32]	Report algorithm, regularization, and interface handling; validate against landmarks or phantoms; interpret layer-specific strain cautiously
Activation versus tissue effect	Post-BTA imaging changes conflate loss of neuromuscular tone with any matrix change	[10, 13, 27, 28]	Add EMG control or matched-activation acquisition and post-washout reassessment
Physiological state	Breathing, Valsalva, contraction intensity, and task alter stiffness/deformation	[1, 7, 19, 26]	Treat loading state as part of the candidate biomarker definition
External load coupling	Pressure-coupled optical/CT/MRI methods improve mechanical interpretation but use specialized setups	[26, 32, 39–45]	Useful for mechanistic validation; current scalability is limited
Cyclic and time-dependent behavior	Studies were built around single maneuvers or two-state comparisons; hysteresis, rate dependence, creep, and change over repeated load cycles were not systematically quantified	Bench context [49, 50]:	Imaging values cannot yet be related to coefficients from cyclic testing; add load-referenced, repeated-cycle protocols

provide objective longitudinal measures after reconstruction. At present, however, these applications remain hypotheses rather than validated decision tools. The literature is fragmented across radiology, surgery, biomechanics, rehabilitation, and engineering, with heterogeneous acquisition protocols and outcome definitions.

Clinical context and potential applications

The clinical need is most evident in ventral and incisional hernia surgery. Decisions such as whether a defect can be closed primarily, whether posterior component separation with transversus abdominis release (TAR) is likely to be required, whether and when to operate after preoperative BTA, how to select mesh, overlap, and fixation, and how to monitor functional recovery currently rest mainly on defect width, defect-to-wall ratios, loss of domain, and surgeon experience [52, 53]. Once validated, imaging-derived mechanical biomarkers could complement these anatomical criteria in three settings: (i) preoperative phenotyping and planning of complex ventral and incisional hernia repair, including monitoring of the response to BTA; (ii) prevention, by identifying patients whose abdominal wall mechanics after laparotomy, stoma formation, or abdominal-flap harvest confer a higher risk of incisional hernia or bulging and who might benefit from tailored closure or prophylactic mesh reinforcement [54], and by providing objective endpoints for trials of closure techniques [8]; and (iii) objective postoperative and rehabilitative follow-up, including diastasis recti. Their relevance to inguinal hernia repair is likely to be more limited: groin hernias arise from a localized weakness of the myopectineal orifice, repair is highly standardized, and outcomes depend predominantly on technique and patient-related factors rather than on global abdominal wall mechanics [55]. Consistent with this, none of the included studies addressed inguinal hernia, although local mechanical characterization of the posterior inguinal wall remains an unexplored research question.

The broader importance of abdominal wall function has recently been underscored by Brucchi et al. [56], who mapped functional assessment around hernia and diastasis surgery using trunk dynamometry, standardized physical tests, and patient-reported outcomes. That synthesis addressed functional and patient-reported assessment rather than imaging-derived candidate

TABLE 3 Candidate clinical applications, candidate biomarkers, current evidence, and evidence gaps (clinician-oriented summary).

Potential application	Candidate biomarker (s)	Current evidence	Potential clinical decision	Key evidence gap
Primary fascial closure/ medialization	Muscle and linea alba stiffness (SWE); pre- to post-BTA stiffness change; MRI/CT deformation and displacement	Preliminary (small, mostly single-center W3/BTA series) [10, 25, 30]	Likelihood of primary closure; anticipated need for TAR or component separation	Prospective link of pre-operative candidate biomarker to intraoperative closure and tension Biomechanical basis: closure tension is a point on the load–elongation relation of the lateral wall, whereas current measures give a tangent stiffness or a strain without load. Needed: load-referenced compliance (force or tension per unit of medial advancement), with and without muscle tone
BTA response monitoring	SWE shear-wave speed/modulus; functional-CT contractility or paralysis grade	Preliminary; within-patient own-control designs [10, 27, 28]	Timing of surgery after BTA; adequacy of chemodenervation	Separating activation from tissue effect; thresholds predicting closure Biomechanical basis: BTA removes the active (contractile) contribution and lowers prestress, moving the operating point toward the toe region; the passive curve itself may be unchanged. Needed: measurements at matched load to separate the two
Individualized operative planning	Rest-Valsalva CT elasticity and orifice distension (GRIP/HEDI); MRI pseudo-compliance	Preliminary; linked research-program cohorts [30–32]	Mesh-defect strategy; fixation; reinforcement location	External, multicenter validation against recurrence and outcomes Biomechanical basis: two-state rest–Valsalva geometry gives strain without measured stress. Needed: Simultaneous pressure measurement to obtain a slope, and linkage to coefficients from cyclic bench testing of the mesh–tissue compound
Mesh selection and sizing	Wall compliance (insufflation/optical); regional strain maps (DIC)	Early/mechanistic; specialized setups [40–42, 45]	Matching mesh stiffness and overlap to wall compliance	Bedside-scalable surrogate; linkage to outcomes Biomechanical basis: requires matching the stress–strain relations of mesh and wall (stiffness, anisotropy, extent of the toe region) over the physiological load range and under repeated load; *in vivo* data cover a limited range, the whole wall, and single cycles
Hernia formation/ recurrence prediction	Layer-specific SWE; linea alba stiffness and distortion; strain heterogeneity	Preliminary; cross-sectional associations only [3, 6, 12]	Risk stratification; intensity of surveillance	Longitudinal cohorts with incident-hernia or recurrence endpoints Biomechanical basis: failure is governed by strength and by fatigue under repeated loading, i.e., by the upper part of the curve and by cyclic behavior, neither of which is sampled *in vivo*; low-load stiffness and strain heterogeneity are indirect surrogates at best

(*Continued*)

TABLE 3 Continued

Potential application	Candidate biomarker (s)	Current evidence	Potential clinical decision	Key evidence gap
Postoperative function and PROMs	Longitudinal SWE and thickness; dynamic-MRI/CT displacement and contour; TDI	Preliminary; longitudinal feasibility [18, 25, 29, 33, 34]	Objective recovery tracking; rehabilitation guidance	Anchoring imaging change to PROMs, trunk performance, return to activity Biomechanical basis: function mainly reflects the active, contractile contribution and whole-wall compliance. Needed: load- and activation-referenced measures that separate active from passive stiffness

All applications are currently supported by preliminary or mechanistic evidence only; the table is intended to prioritize validation research, not to endorse clinical use. Bracketed numbers refer to the reference list. BTA, botulinum toxin A; CT, computed tomography; DIC, digital image correlation; DIEP/DIEAP, deep inferior epigastric perforator/artery perforator; MRI, magnetic resonance imaging; PROMs, patient-reported outcome measures; SWE, shear-wave elastography; TAR, transversus abdominis release; TDI, tissue deformation index.
Linked, potentially non-independent reports cited in this table: [25–28]; [30–32]; [3, 6]. For each application, a candidate biomarker would also need to show incremental value over established patient-, disease-, and surgeon-related predictors before influencing clinical decisions. "Biomechanical basis" relates each evidence gap to the stress–strain relationship (Figure 1) and to cyclic, time-dependent behavior; candidate biomarkers are used in the sense defined in the Introduction.

mechanical biomarkers. A focused mapping of quantitative candidate imaging biomarkers used to characterize abdominal wall mechanical function *in vivo* therefore remains needed.

Methods

Review design, framework, and reporting

A scoping review was selected because the available literature spans heterogeneous imaging modalities, populations, acquisition paradigms, biomechanical constructs, and clinical applications that are not expected to support conventional pooled meta-analysis. The review followed the framework proposed by Arksey and O'Malley [57], refinements by Levac et al. [58], updated JBI guidance [59], and the PRISMA extension for Scoping Reviews (PRISMA-ScR) [60]. The choice of a scoping rather than systematic-effect review was consistent with established guidance [61]. The review objectives, eligibility criteria, and data-charting structure were defined *a priori*, before title/abstract screening and full-text charting. Following the initial searches, two prespecified-in-principle refinements were applied: Web of Science was added as a third source, and optical, photogrammetric, and indentation-based surface-mechanics methods yielding quantitative wall-mechanics endpoints were explicitly included; the core Population-Concept-Context definitions were not otherwise changed.

The review question was: which *in vivo* imaging techniques have been used to quantitatively characterize abdominal wall mechanical function, which candidate biomarkers do they generate, and how have these measurements been applied to abdominal wall surgery and related conditions?

Eligibility criteria (PCC framework)

Population

Adults or children undergoing imaging of the abdominal wall, including healthy volunteers, patients with ventral or incisional hernia, diastasis recti abdominis (DRA), or cohorts undergoing abdominal wall surgery or abdominal wall tissue harvest. Abdominal-wall tissue-harvest cohorts (e.g., DIEP/DIEAP or TRAM abdominal-flap donor sites) were included *a priori* because they undergo standardized pre- and post-harvest quantitative imaging of the same rectus and lateral wall structures, providing within-subject, longitudinal measurements of donor-site mechanical function that are directly relevant to abdominal-wall integrity.

Concept

In-vivo imaging that generated at least one quantitative candidate biomarker of abdominal wall mechanical function or tissue biomechanical behavior, including stiffness/elasticity, shear-wave speed or modulus, deformation, strain, displacement, contractility, compliance, dynamic muscle thickness/length, or stress-dependent contour/bulging metrics. In keeping with the three-level terminology set out in the Introduction, these outputs are referred to as candidate biomarkers, i.e., measured quantities or derived mechanical parameters proposed, but not yet clinically qualified, as indicators of abdominal wall status.

Context

Physiological activation or loading (e.g., rest versus contraction, breathing, coughing, Valsalva, abdominal inflation, crunch, electrical stimulation, external loading) or longitudinal assessment before/after an intervention such as BTA injection or surgery.

Operational definition of imaging

For this review, imaging was defined broadly as any *in vivo* technique producing a spatially resolved or image-based quantitative measurement of abdominal-wall mechanical behavior. This encompassed clinical cross-sectional and ultrasound modalities (SWE/ARFI, dynamic or cine MRI, functional or stress CT, and dynamic B-/M-mode ultrasound) and optical, photogrammetric, and indentation-based surface-

mechanics methods, which reconstruct wall geometry, displacement, or strain from image data (e.g., three-dimensional laser scanning, stereophotogrammetry, digital image correlation, or optical/time-of-flight displacement sensing). Non-imaging biomechanical techniques that did not generate spatially resolved image data (e.g., isolated trunk dynamometry, surface electromyography without concurrent imaging, or pressure catheters used alone) were not eligible on their own, but were retained when combined with an eligible imaging method (e.g., pressure-referenced dynamic MRI or insufflation-coupled photogrammetry). The seven surface-mechanics studies are, at present, research and mechanistic tools rather than bedside modalities; their principal value here is to provide load-referenced, patient-specific constitutive information against which the more clinically deployable ultrasound, MRI, and CT candidate biomarkers can be interpreted and calibrated.

Eligible modalities included SWE, ARFI or related ultrasound elastography, dynamic or cine MRI when used to quantify wall motion/deformation, functional CT, Valsalva CT when linked to mechanical/functional wall metrics, and dynamic ultrasound/myosonography.

Studies were excluded when imaging was used solely for diagnostic detection or visibility of hernia, adhesion mapping, mesh visualization, or qualitative mobility/dysmotility without a quantitative mechanical or functional endpoint. Animal-only studies, reviews, and case reports without quantitative wall biomechanics, and studies focused on non-abdominal-wall organs, were excluded. The operational boundary was whether the imaging output itself quantified a mechanical or functional property of the wall under a defined state or load. Thus, a Valsalva CT study reporting only improved hernia visibility or sac size was excluded, whereas rest-versus-Valsalva CT was eligible when used to quantify tissue elasticity, instability, displacement, strain, or stress-dependent wall geometry.

Information sources and search strategy

PubMed/MEDLINE was searched on 16 August 2026, and Embase and Web of Science on 17 August 2026. These dates denote the final execution of each database search for the included set. Search concepts combined abdominal wall/abdominal muscle/ventral or incisional hernia/linea alba/rectus abdominis/diastasis terms with elastography, shear-wave, dynamic MRI, functional or Valsalva CT, deformation, displacement, strain, stiffness, contractility, compliance, and related terms. PubMed yielded 83 records and Embase 1,154 records; 66 Embase records duplicated PubMed records (Section *Selection of sources of evidence*). Web of Science returned 755 records, of which 754 were available for screening (one record could not be exported). The full reproducible search syntax for all three databases is provided in Supplementary Table S1. Web of Science was searched in addition to PubMed/MEDLINE and Embase because it more completely indexes engineering, biomechanics, and applied-physics journals (e.g., Journal of the Mechanical Behavior of Biomedical Materials, Computer Methods and Programs in Biomedicine, Sensors, and Frontiers in Bioengineering and Biotechnology) that are only partially covered by the biomedical MeSH/Emtree indexing of the other two databases. Consistent with this, the records uniquely retrieved through Web of Science were predominantly engineering and biomechanics reports rather than clinical studies. Backward and forward citation searching (reference-list screening of included reports and forward citation tracking) was also performed; the number of additional eligible reports identified through this step is reported in the flow diagram (Figure 2).

Selection of sources of evidence

Records from the three databases were handled within a single, consolidated selection funnel (Figure 2). In total, 1,992 records were identified (PubMed/MEDLINE 83; Embase 1,154; Web of Science 755), of which one Web of Science record could not be exported because of a platform export failure. Cross-database duplicates were identified across the complete exports of all three sources by DOI, PMID, and normalized title, with title verification of every DOI match (several conference abstracts share a supplement-level DOI): 66 PubMed/MEDLINE records were also retrieved by Embase, and 98 Web of Science records duplicated records retrieved from PubMed/MEDLINE or Embase. After removal of these 164 duplicates, 1,827 unique records underwent title/abstract screening, of which 1,773 were excluded. Fifty-four reports were sought for full-text assessment; two could not be retrieved, 52 were assessed, seven were excluded (no quantitative mechanical endpoint, n = 3; conference abstract only, n = 1; German-language full text that could not be reliably assessed, n = 2; non-peer-reviewed preprint, n = 1), and 45 reports were included. Because Web of Science was added after the initial PubMed/MEDLINE–Embase search (Section *Review design, framework, and reporting*), its records were screened in a second round against the same prespecified PCC criteria. During the original screening rounds, duplicates had been identified only against already-included studies, so some duplicate records were screened more than once; the complete cross-database deduplication reported above was therefore performed retrospectively for this revision. Screening decisions were concordant for all duplicate pairs except one: the report by Chino et al. [21] was excluded at title/abstract in the Embase round and included on re-screening of its Web of Science record. The source database of each included report is indicated in Supplementary Table S3. For the two reports that could not be retrieved (one from Embase and one from Web of Science), we attempted institutional full-text access, interlibrary loan, preprint- and institutional-repository searches, and direct author contact, without success. On the basis of their titles and abstracts, these two records did not describe modalities, candidate biomarkers, or populations absent from the included set, so their unavailability is unlikely to alter the evidence map; of the 17 full-text reports retrieved only through Web of Science, 16 met the prespecified PCC criteria and one, a non-peer-reviewed preprint, was excluded. Several included reports originated from the same research groups and may share participants or control groups: the Kallinowski/GRIP/HEDI program [30–32]; the BTA/functional-CT reports by Tomazini Martins et al. and Read et al. [27, 28]; the dynamic-MRI reports by Jourdan et al. and Joppin et al. [23–26]; the SWE reports by Wang et al. and He

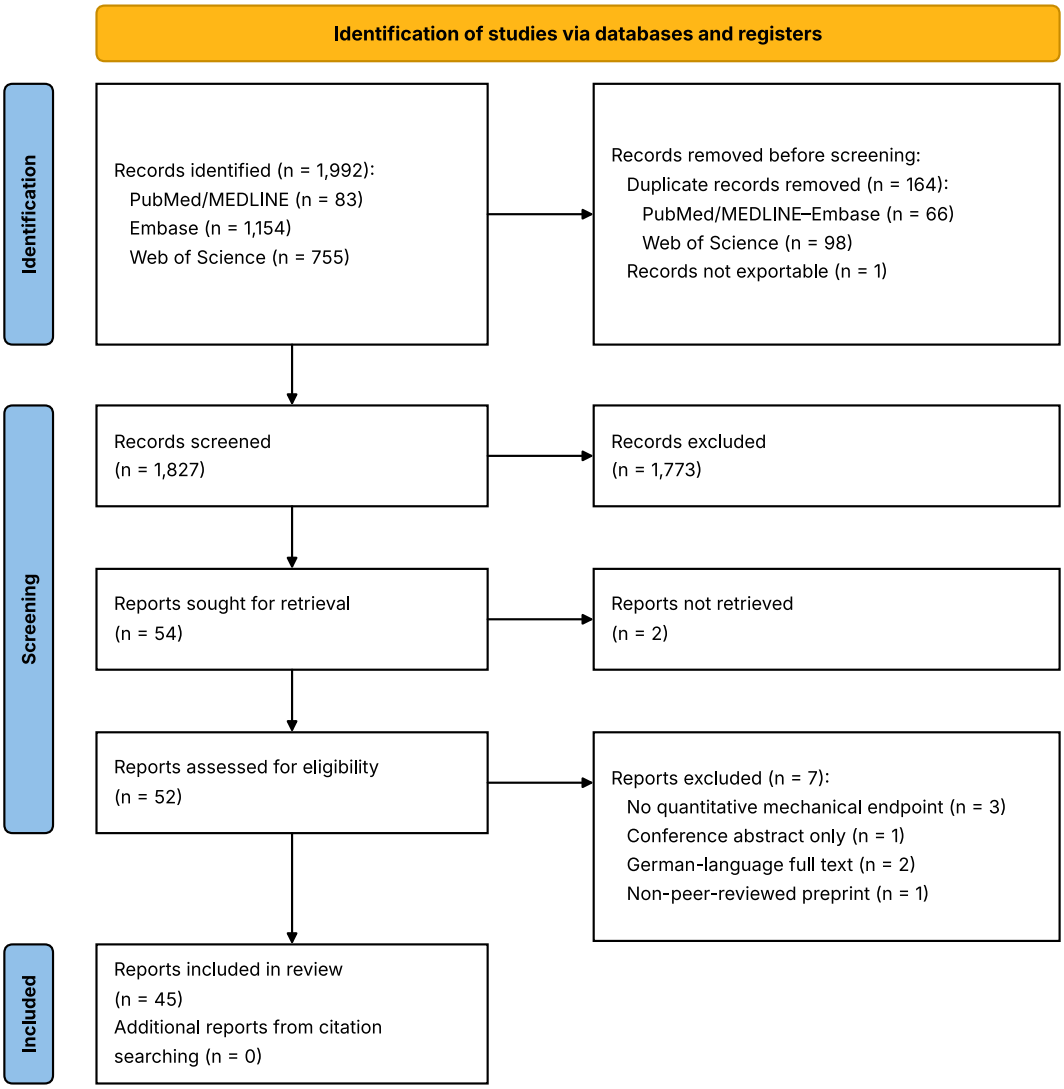


FIGURE 2
PRISMA-ScR flow diagram of study identification and selection, consolidated across PubMed/MEDLINE, Embase, and Web of Science. Records identified: 1,992 (PubMed/MEDLINE 83; Embase 1,154; Web of Science 755; one Web of Science record not exportable). Cross-database duplicates removed: 164 (66 PubMed/MEDLINE–Embase; 98 Web of Science). Records screened: 1,827; excluded at title/abstract: 1,773. Reports sought: 54; not retrieved: 2; assessed: 52; excluded: 7 (no quantitative mechanical endpoint, 3; conference abstract, 1; German-language full text, 2; preprint, 1); included: 45. Web of Science records were screened in a second round against the same criteria; deduplication across complete exports was performed retrospectively. Linked reports from shared research programs are identified in Table 1; Supplementary Table S3.

et al. [3, 4, 6]; the M-mode TDI reports by Biały et al. [35, 36]; and the photogrammetric reports by Lubowiecka et al. and Troka et al. [41, 45]. These were retained as distinct reports when they contributed non-identical methods or outcomes, but were treated as potentially non-independent evidence: they are flagged in Tables 1,3 and in Supplementary Table S3, and participant numbers were not summed across them. Representative borderline exclusions and the operational rationale are provided in Supplementary Table S2.

Title/abstract screening, full-text eligibility assessment, and data charting were conducted independently by two reviewers (FB and RS), who were blinded to each other's decisions during the review process, using the prespecified PCC criteria and a structured charting form. Records considered borderline were re-evaluated against the operational definition of a quantitative mechanical/functional endpoint before a final decision.

Data charting and synthesis of results

For each included study, the following items were charted on a piloted form: publication year, design, population and sample size, clinical condition or surgical context, imaging modality, activation/loading paradigm, structures assessed, candidate biomarker and unit, principal imaging-derived findings, proposed clinical application, and measurement-property features relevant to interpretation (including repeatability, observer dependence, probe pressure, acquisition plane, depth/layer effects, and task standardization when reported). Because the included studies

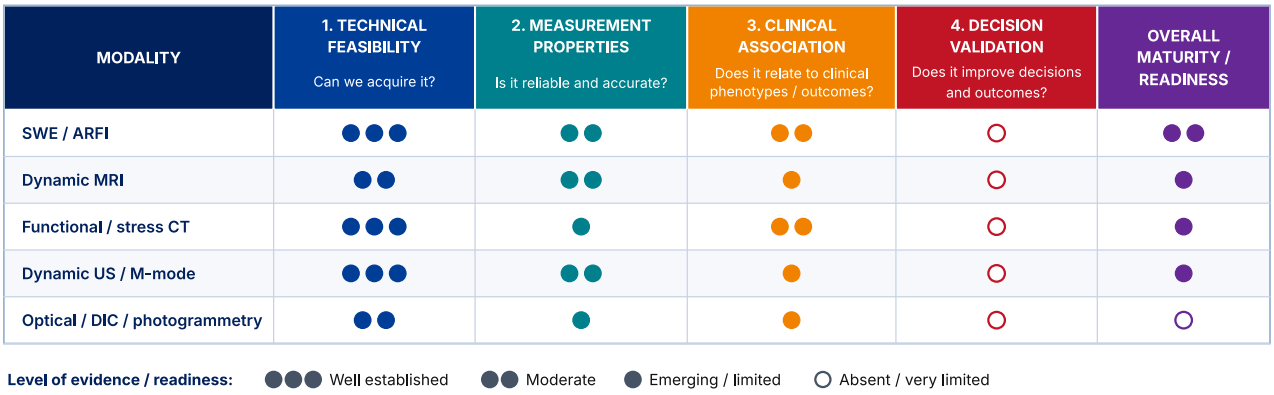


FIGURE 3
Evidence maturity map from technical feasibility to clinical decision support. Conceptual evidence-maturity map derived from the scoping synthesis. Filled symbols indicate the relative depth of evidence within each domain rather than a formal quality score or risk-of-bias rating. Ratings (well established/moderate/emerging or limited/absent or very limited) were assigned by two reviewers using the explicit, pre-specified descriptors defined in Methods (section *Data charting and synthesis of results*) and detailed in Supplementary Table S4, and reflect the concentration of evidence within each translational domain rather than a validated grading of study quality. Across modalities, technical feasibility is generally established or emerging, whereas measurement properties and clinical associations remain heterogeneous and prospective decision validation is absent or very limited. The map therefore illustrates the translational gap between the ability to measure abdominal-wall biomechanics and the ability to use those measurements to improve clinical decisions or outcomes. ARFI, acoustic radiation force impulse; CT, computed tomography; DIC, digital image correlation; MRI, magnetic resonance imaging; SWE, shear-wave elastography; US, ultrasound.

report different mechanical quantities, we additionally charted, for each report, the parameter actually measured (e.g., shear-wave speed) versus parameters derived from it (shear or Young's modulus) or obtained by other methods (e.g., force–displacement structural stiffness by indentation), the formula or device output used for the derivation, the imaging plane and probe orientation relative to fiber direction, and the loading or activation state at acquisition. Because of marked heterogeneity, findings were synthesized narratively by imaging family and mapped across a common five-element structure (modality, loading maneuver, structure/ROI, candidate biomarker/unit, and clinical linkage). Consistent with JBI and PRISMA-ScR guidance, and because the objective was to map the extent and nature of the evidence rather than to estimate a pooled effect, a formal study-level risk-of-bias instrument was not applied. Instead, we performed a structured appraisal of measurement properties and the principal sources of technical uncertainty for every modality (repeatability/reliability, probe-pressure effects, imaging-plane/anisotropy, layer/depth effects, physiological state, and external-load coupling), summarized in Table 2. Sample sizes were not summed across potentially overlapping reports.

Evidence-maturity mapping

To make the conceptual synthesis transparent, each imaging family was rated across four translational domains, technical feasibility, measurement properties (reliability and measurement error), clinical association, and prospective decision validation, using pre-specified qualitative descriptors applied independently by two reviewers (FB, RS) and reconciled by discussion (Figure 3). For each domain a family was rated as well established (multiple independent studies, including patient cohorts, with reproducibility data and/or external replication), moderate (two or more studies with consistent findings but limited reproducibility or external validation), emerging or limited (single or few small or healthy-volunteer/feasibility studies), or absent or very limited (no eligible study addressing that domain). These descriptors are explicitly qualitative and reviewer-derived; they do not constitute a validated grading system (e.g., GRADE) or a quantitative quality score. Figure 3 should therefore be read as a conceptual map of where evidence is concentrated and where it is missing, chiefly the translational gap at the level of prospective decision validation, rather than as a formal quality appraisal. The full domain-by-family ratings with their justifications are provided in Supplementary Table S4.

Results

Study selection and overall characteristics

Forty-five reports published between 1986 and 2026 met the current eligibility criteria (Figure 2); full per-study characteristics are provided in Supplementary Table S3. Twenty-two used SWE, ARFI, or related elastographic methods; four used dynamic MRI; six used functional or stress CT; six used dynamic ultrasound or M-mode myosonography; and seven used optical, photogrammetric, or indentation-based surface-mechanics methods. Study populations ranged from healthy volunteers used for normative, reliability, or mechanistic characterization to patients with incisional or ventral hernia, pregnancy-related or postpartum DRA, obesity, complex hernia undergoing BTA, patients after eTEP reconstruction, children after transverse laparotomy closure, women after lipoabdominoplasty, abdominal-flap breast reconstruction cohorts, patients undergoing laparoscopic insufflation, peritoneal-

dialysis patients, and individuals with tetraplegia. The expanded evidence base includes time-resolved muscle deformation, contraction-related thickness change, pressure-volume compliance, three-dimensional surface strain, stress-strain-derived stiffness, probe- and plane-dependent SWE measurement effects, and inverse-FEA material characterization.

Ultrasound elastography and ARFI: stiffness as a candidate imaging biomarker

Mechanical parameters, direction, and testing conditions

Because the studies in this section report different quantities, these are distinguished explicitly here and in Table 1. SWE and ARFI do not measure stiffness directly: an acoustic radiation-force push generates a small-amplitude shear wave, and the system reports its propagation speed (c, in m/s) in the imaging plane, i.e., along the long axis of the transducer. In all included SWE/ARFI studies acquisition was performed *in vivo* without a controlled external load; the only "loading condition" was the physiological state at the time of acquisition (rest, breathing phase, voluntary contraction, Valsalva, active abdominal inflation, or neuromuscular stimulation), and intra-abdominal pressure was not measured. Shear modulus (μ, kPa) is then derived as $\mu = \rho c^2$, assuming a tissue density $\rho \approx 1{,}000\ kg/m^3$, and Young's modulus (E, kPa) as $E \approx 3\mu$. Some systems display E by default, and several studies report the output generically as "stiffness" or "elasticity", so kPa values from different studies may correspond to μ or to E and are not interchangeable (a three-fold difference). All of these are small-strain, apparent (tangent) moduli at the prevailing state of prestress, measured along the probe direction; they are not the large-strain, direction-specific properties obtained by uniaxial or biaxial tensile testing of excised tissue. Probe orientation was specified in 18 of the 22 SWE/ARFI reports: aligned with the fibers of the imaged muscle in seven [2, 8, 11, 13, 16, 19, 22], transverse to the body axis without reference to fiber direction in seven [3, 4, 6, 9, 14, 15, 18], longitudinal in one [17], and in both orientations in three [1, 7, 21]; it was not stated in four [5, 10, 12, 20] (Supplementary Table S3). This matters because shear-wave speed in muscle is anisotropic [21, 62]. Likewise, ten reports expressed results as shear-wave speed (m/s), five as shear modulus [1, 11, 16, 19, 22], three as Young's modulus [10, 14, 17], and four as "stiffness" or "elasticity" without specifying the modulus [9, 12, 18, 20]. These SWE-derived parameters are distinct from the "local abdominal stiffness" reported by Tran et al. [1] and from the structural stiffness reported in surface-mechanics studies (Section *Optical/photogrammetric pressure-deformation imaging*), which were obtained by applying a low external force to the abdominal surface (indentation) and are expressed as force per unit displacement (N/mm): they describe the structural response of the whole multilayer wall at that site rather than a material modulus of an individual layer.

The largest body of evidence addressed tissue stiffness. Tran et al. [1] characterized the anterolateral abdominal wall in healthy volunteers using SWE during rest, abdominal breathing, pullback loading, and Valsalva. Valsalva increased muscle shear modulus, while local abdominal stiffness also changed with activity (shear modulus derived from SWE, kPa; local stiffness measured separately by low-load indentation of the abdominal surface, N/mm), establishing that elastographic measurements are state-dependent rather than fixed tissue attributes.

Gabrielsen et al. [2] evaluated ARFI-derived shear-wave velocity and sonographic texture features as quantitative candidate biomarkers of abdominal wall muscle properties. Their pilot work supported feasibility and reliability but also emphasized the need to control subject- and technique-related factors. This issue was explored more directly by Zemzemi et al. [5], who demonstrated that layered abdominal wall structures can introduce important shear-wave measurement biases and that wave-propagation assumptions may not always be valid. These methodological observations are central to interpretation of apparently precise stiffness values.

Which assumptions are questionable, and at which step

Estimating elasticity by SWE involves three steps, each relying on assumptions that are only partly met in the abdominal wall. (i) *Measurement of shear-wave speed* assumes a bulk shear wave traveling through a locally homogeneous, effectively semi-infinite medium. This is reasonable in a thick muscle belly but not in thin structures such as the linea alba, the rectus sheath, the oblique aponeuroses, or a thin transversus abdominis: when layer thickness is comparable to or smaller than the shear wavelength, the wave is guided by the layer boundaries (Lamb-type, dispersive propagation), so the measured speed depends on thickness and frequency and no longer reflects the bulk shear-wave speed [5, 63]. Zemzemi et al. showed that the wave field is then dominated by the antisymmetric (A0) Lamb mode, leading to underestimation of shear-wave speed in muscle and skin layers and overestimation in fat; *in vivo*, the shear wavelength exceeded layer thickness in both muscle (≈14 vs. 10 mm) and the linea alba (≈34 vs. 5 mm) [5]. Interfaces between layers with different properties further distort the wave field, and deep layers are affected by attenuation and lower signal-to-noise ratio [5, 11]. (ii) *Conversion of speed to shear modulus* ($\mu = \rho c^2$) assumes a linear-elastic, isotropic, non-viscous medium. Skeletal muscle and aponeurosis are transversely isotropic, so speed and the derived μ depend on the angle between the wave and the fibers [21, 62]; viscosity makes speed frequency-dependent; and, importantly, abdominal wall tissues are nonlinear (strain-stiffening) and prestressed by intra-abdominal pressure and muscle activation. Under prestress, shear-wave speed rises with tensile stress along the propagation direction (acoustoelastic effect) [64], so an increase in speed during Valsalva, abdominal inflation, or contraction largely reflects increased tension and geometric loading of the wall rather than a change in intrinsic tissue properties. (iii) *Conversion of μ to Young's modulus* ($E \approx 3\mu$) additionally assumes isotropy and incompressibility and therefore does not yield the tensile modulus of anisotropic tissue in either the fiber or the cross-fiber direction. These assumptions are most defensible for shear-wave speed itself, measured in thick muscle at rest with a standardized probe orientation, and least defensible for thin aponeurotic structures, deep layers, and acquisitions under high, unmeasured intra-abdominal pressure. Consequently, SWE

outputs in the abdominal wall should be interpreted as state-, direction-, and protocol-specific measures of apparent stiffness under the prevailing load, not as intrinsic, load-independent material constants.

Clinical case-control studies consistently suggested that hernia is associated with altered abdominal muscle stiffness. Wang et al. [3] reported significantly higher shear-wave speed in the rectus abdominis, external oblique, internal oblique, and transversus abdominis in patients with incisional hernia compared with healthy controls. A subsequent study in 53 women with incisional hernia found that shear-wave speed of several lateral abdominal muscles increased with greater hernia width, whereas muscle thickness was a less reliable marker of biomechanical change. In postpartum DRA, He et al. [4] likewise demonstrated altered shear-wave speed patterns relative to healthy controls and associations between selected elastographic measurements and inter-rectus distance. Because neither muscle activation nor intra-abdominal pressure was measured in these case-control studies, part of the observed differences may reflect differences in resting tone or wall tension rather than intrinsic tissue properties.

Other studies extended elastography from disease characterization to physiological and interventional assessment. Vergari et al. [7] developed a standardized protocol for linea alba SWE and showed that active abdominal inflation markedly increased shear-wave speed, while normal breathing had a smaller effect; their protocol improved reproducibility compared with previous approaches. Short et al. [9] used isolated neuromuscular stimulation of the pyramidalis and demonstrated an increase in linea alba SWE-derived elasticity from 15.7 to 24.2 kPa during contraction, providing mechanistic evidence that local muscle activation alters aponeurotic stiffness.

Two recent studies illustrated potential perioperative applications. Shehata et al. [8] used ultrasound and elastography as objective tissue-healing outcomes after a randomized pediatric transverse laparotomy closure trial and found greater stiffness and structural abnormalities after mass closure than layer-by-layer closure. Most directly relevant to complex hernia reconstruction, Rajabzoda et al. [10] evaluated six W3 ventral hernia patients longitudinally and found markedly elevated pre-BTA stiffness, substantial reduction after BTA, and progressive postoperative reductions through 12 months after Rives–Stoppa repair. Although clinically compelling, the very small treated sample precludes validated thresholds or prognostic claims. Moreover, as discussed in Section *Discussion*, post-BTA reductions in shear-wave speed are likely to reflect, at least in part, abolished neuromuscular tone rather than remodeling of the tissue itself.

MacDonald et al. [11] demonstrated fair-to-excellent intra-session and inter-rater reliability of abdominal muscle shear modulus during hollowing and bracing, while also showing reduced measurement success and reliability in deeper muscles. Chino et al. [13] used SWE during trunk rotation to demonstrate activation-dependent changes in external and internal oblique shear-wave velocity and to interrogate surface-EMG crosstalk. Kozawa et al. [19] extended this concept to graded abdominal draw-in intensity, showing region-specific increases in TrA and IO shear modulus with increasing task intensity. Beamish et al. [12] showed that women with DRA had lower linea alba stiffness and greater task-related distortion than women without DRA, supporting the concept that IRD alone incompletely represents linea alba mechanical behavior. More recent pregnancy and postpartum studies by Guo et al. [14] and Wang et al. [17] combined two-dimensional ultrasound with SWE to track IRD, rectus thickness, and Young's modulus across gestation and postpartum, while Kumar et al. [15] provided reference SWE and thickness measurements in multiparous women. Lim et al. [16] demonstrated age-related differences in TrA stiffness and its loading-dependent relationship with expiratory function. Bielaczyc and Simka [20] further explored linea alba and fascial mechanics during Valsalva, curl-up, and side-plank tasks in normal-weight and obese adults. Finally, Zhou et al. [18] demonstrated longitudinal increases in the elasticity of abdominal skin, subcutaneous tissue, rectus abdominis, and external oblique 6 months after lipoabdominoplasty. Collectively, these studies reinforce both the biological sensitivity of SWE and the importance of standardized task, depth, body habitus, and region-of-interest definitions.

Measurement-method studies further qualify interpretation of apparently precise SWE values. Chino et al. [21] showed that imaging plane changes image stability and can alter measured shear-wave velocity, supporting explicit consideration of muscle-fiber orientation and anisotropy. Mikołajowski et al. [22] demonstrated that uncontrolled probe compression can underestimate lateral abdominal muscle thickness and overestimate shear modulus; force-controlled acquisition reduced smallest detectable differences. Together with the depth/layer limitations described by Zemzemi et al. [5] and reduced deep-muscle reliability reported by MacDonald et al. [11], these findings argue against treating stiffness values as device-independent or protocol-independent biomarkers.

Dynamic MRI: deformation, displacement, and pressure-motion coupling

Dynamic MRI provided the most detailed whole-wall measurements of movement and deformation. Jourdan et al. [23] first developed a semiautomatic image-registration approach that quantified spatial and temporal deformation of abdominal wall muscles during controlled breathing. The method achieved high segmentation and registration correspondence and established a framework for regional rather than purely global assessment. Regional strain estimates obtained by deformable image registration are, however, sensitive to how the algorithm handles sliding fascial interfaces (Section *Measurement properties and sources of uncertainty*).

In a subsequent study of 20 healthy volunteers, the same group [24] quantified abdominal wall behavior during forced breathing, coughing, and Valsalva. Circumferential and radial strains, muscle length and thickness changes, and regional radial displacement were calculated. Lateral abdominal muscles displayed greater deformation than the rectus abdominis, and the magnitude and direction of displacement depended on both region and maneuver, demonstrating that 'abdominal wall function' cannot be represented by a single scalar measurement.

Joppin et al. [26] extended this framework by simultaneously measuring dynamic MRI displacement and intra-abdominal pressure using an ingestible pressure sensor. Strong pressure-

displacement relationships were observed, but they were muscle-, task-, and participant-specific. Abdominal pseudo-compliance showed substantial inter-individual variability, supporting the concept that mechanical phenotype may be patient-specific and that motion cannot be interpreted independently of the loading condition.

The strongest direct surgical evidence came from a prospective pre/post study by Joppin et al. [25] of 11 patients undergoing ventral hernia repair with mesh. Dynamic MRI during breathing, coughing, and Valsalva quantified changes in the hernia sac, inter-recti distance, muscle geometry, and regional displacement. Postoperative imaging demonstrated measurable changes in muscle length and motion as well as a reduction in inter-recti distance, but with marked inter-individual variability. The study establishes the feasibility of longitudinal biomechanical imaging after reconstruction, while also highlighting the need for larger cohorts linked to recurrence, symptoms, and function.

Functional and stress CT: contractility, BTA response, and postoperative geometry

Functional CT studies used active contraction or stress imaging to move beyond static cross-sectional anatomy. Tomazini Martins et al. [27] compared functional CT with single-point electromyography in selected high-risk patients after BTA-assisted ventral hernia repair. CT demonstrated heterogeneous and sometimes incomplete paralysis across abdominal muscle segments and changing treatment effects over time, whereas electromyography showed limited diagnostic performance against the CT reference. These data suggest that functional imaging may reveal spatial heterogeneity that single-point physiological tests miss.

Read et al. [28] described a 'functional CT' approach supplementing resting imaging with a strong abdominal crunch. In a large observational experience, contraction images were used to improve characterization of complex ventral hernias, distinguish true hernia from dysfunctional bulging, identify denervation or atrophic change, and assess BTA-related functional effects. The study is clinically influential but is a descriptive Hypothesis and Theory report rather than a conventional comparative study and may overlap with related Australian BTA cohorts; its sample should therefore not be double-counted in quantitative summaries.

Daes et al. [29] applied CT-based metrics after eTEP repair for small ventral hernia with diastasis recti. Abdominal contour, semilunar-line distance, rectus width and area, and a mathematical bulging metric were assessed, with Valsalva used in a subgroup. Bulging was more common under stress than on non-stressed imaging, and postoperative geometry changed after reconstruction. The study also explored rehabilitation, suggesting that imaging can be used not only for surgical anatomy but also to quantify functional recovery, although its retrospective quality-improvement design limits causal interpretation.

Kallinowski et al. [30] added a complementary patient-specific biomechanical application of stress CT. Preoperative CT at rest and during Valsalva was used to estimate abdominal wall tissue elasticity and hernia-orifice distension, with these measurements incorporated into a reconstruction strategy together with mesh and fixation characteristics. Although the study combined imaging with bench testing and clinical implementation rather than validating a stand-alone CT biomarker, it illustrates how stress-dependent geometry may be translated directly into individualized operative planning.

A related study, the GRIP report [31] combined rest/Valsalva CT assessment of defect expansion and tissue elasticity with bench-derived CRIP/GRIP concepts and a multicenter clinical implementation cohort. More recently, Lösel et al. [32] introduced HEDI, an automated CT-based workflow that registers rest and Valsalva acquisitions to map displacement and Green-Lagrange strain, segment hernia and abdominal-wall structures, and visualize areas of mechanical instability. These reports extend stress CT from descriptive geometry toward explicit patient-specific biomechanical planning, but they arise from an overlapping research program and should be interpreted as linked methodological/clinical reports rather than independent participant samples.

Dynamic myosonography

Dynamic ultrasound studies quantified muscle behavior from contraction-related thickness change or time-resolved deformation. Lee et al. [34] assessed rectus abdominis thickness and contractility before DIEP flap harvest and at 1 month and 1 year, showing transient postoperative thickening but preserved contractility. Seidenstuecker et al. [33] similarly used myosonography to measure rectus abdominis thickness at rest and during maximal contraction before and after abdominal-flap breast reconstruction, demonstrating better postoperative function after DIEAP than muscle-sparing TRAM harvest. Biały et al. [35] introduced an M-mode tissue deformation index (TDI), defined as the percentage change in lateral abdominal muscle thickness over time during rapid loaded arm abduction; in 34 healthy volunteers, three repeated measurements achieved good intra-rater reliability. A later study in 126 healthy volunteers [36] confirmed a characteristic deep-to-superficial TDI gradient and identified side-to-side asymmetry predominantly in transversus abdominis. Together, these studies show that conventional ultrasound can provide quantitative dynamic candidate biomarkers beyond static thickness, although task standardization, between-rater reproducibility, and clinical validation remain limited. Brown and McGill [37] used ultrasound to track *in vivo* deformation of rectus-sheath and oblique aponeurotic connective tissues during graded contraction, demonstrating complex multiplanar deformation and lateral rectus movement. Vasseljen et al. [38] compared high-temporal-resolution M-mode and tissue-velocity-derived ultrasound strain rate with intramuscular EMG during rapid arm flexion, showing that ultrasound can quantify the timing and rate of deformation in layered abdominal muscles.

Optical/photogrammetric pressure-deformation imaging

Optical, photogrammetric, and indentation-based methods extend quantitative functional imaging from internal tissue properties to whole-wall surface mechanics under defined loading. Goldman et al. [39] related gastric pressure to

abdominal volume displacement obtained with optical contour mapping during passive expiration. Song et al. [40] tracked infrared surface markers during laparoscopic insufflation and combined three-dimensional displacement with ultrasound-measured wall thickness to derive stress, strain, and Young's modulus. Becker et al. [42] similarly synchronized video-derived sagittal strain with insufflator pressure in 25 laparoscopic patients to derive individual abdominal-wall compliance. Todros et al. [43] used repeated 3D laser scans in relaxed and maximally contracted states to map surface displacement with sub-percent acquisition variability. Lubowiecka et al. [41] used multi-view photogrammetry during peritoneal dialysis with measured intra-abdominal pressure to calculate patient-specific principal strain fields and directions. Troka et al. [45] subsequently applied digital image correlation and self-organizing maps to full-field pressure-dependent strain data, identifying regions with similar mechanical behavior across the abdominal surface. Remus et al. [44] combined controlled macro-indentation with time-of-flight optical 3D displacement sensing and inverse finite-element analysis to derive region- and activation-dependent hyperelastic material parameters. Although technically heterogeneous, these approaches share a major biomechanical advantage: deformation is interpreted relative to an imposed or measured load, moving closer to direct characterization of compliance, anisotropy, and patient-specific constitutive behavior.

Cross-cutting methodological heterogeneity

Across modalities, heterogeneity was substantial. Loading conditions included quiet breathing, passive expiration, forced breathing, cough, Valsalva, abdominal inflation, laparoscopic insufflation, peritoneal-dialysis filling, crunch, electrical stimulation, maximal voluntary contraction, and external loading. Some studies measured passive resting stiffness, whereas others measured changes between activation states or explicitly coupled deformation to pressure. Structures ranged from the linea alba and individual muscle layers to whole-wall contour and hernia-sac geometry. Candidate biomarkers were reported in m/s, kPa, N/mm, millimeters of displacement, percent strain, muscle length or thickness change, TDI (%/ms), pressure-volume compliance, semi-quantitative contractility grades, and derived compliance indices. These units denote different physical quantities: m/s is the primary SWE measurement (shear-wave speed); kPa denotes model-derived shear modulus (μ) or Young's modulus ($E \approx 3\mu$), which differ three-fold and depend on the assumptions discussed in Section *Ultrasound elastography and ARFI: stiffness as a candidate imaging biomarker*; and N/mm denotes structural force–displacement stiffness of the whole wall, which is not comparable with either. Table 1 now reports measured and derived quantities separately. Very few candidate biomarkers were externally validated against clinically meaningful endpoints, and reproducibility was inconsistently reported. Table 1 summarizes this landscape by imaging family. Cross-cutting measurement properties and the principal sources of bias and measurement error are summarized in Table 2.

Measurement properties and sources of uncertainty

Across the evidence base, reliability and measurement error were reported inconsistently and were usually examined in small methodological cohorts. Repeated-measure studies support acceptable within-session reliability for selected SWE and M-mode metrics [2, 7, 11, 35, 36], but reliability is not uniform across deeper muscle layers [11]. Acquisition geometry is a major source of variation: SWE values can depend on imaging plane and fiber orientation [21], probe compression [22], and layered-wave propagation assumptions [5]. Functional candidate biomarkers are also state-dependent, changing with breathing phase, Valsalva, contraction intensity, position, and task instruction [1, 7, 19, 26]. Dynamic ultrasound timing and deformation metrics require high temporal resolution and task standardization [35, 36, 38]. Optical and pressure-coupled methods provide direct mechanical loading information but rely on specialized setups and small cohorts [39–45]. Accordingly, current values should be interpreted as protocol-specific measurements rather than transferable clinical thresholds. Elastographic values are additionally load-dependent because of tissue nonlinearity and prestress (Section *Ultrasound elastography and ARFI: stiffness as a candidate imaging biomarker*).

Registration-derived displacement and strain

The regional displacement and strain fields reported by dynamic MRI [23–26] and stress CT [32] are not measured directly but are computed by deformable image registration (DIR; e.g., diffeomorphic registration with B-spline regularization, as in [23], or demons and optical-flow algorithms) between consecutive frames or between rest and Valsalva acquisitions. Most DIR algorithms impose a smoothness (regularization) constraint on the displacement field. The abdominal wall, however, consists of layers that slide relative to each other along loose fascial planes (e.g., between the external oblique, internal oblique, and transversus abdominis, and between the wall and the viscera), producing discontinuities in tangential displacement. Smoothness regularization across these interfaces suppresses interlayer slip and redistributes it as spurious shear strain within adjacent muscles; because strain is the spatial derivative of displacement, such errors are amplified in strain maps [65]. Interface-preserving approaches (layer-wise or segmentation-guided registration and direction-dependent, sliding-preserving regularization) and validation against tracked anatomical landmarks or phantoms can mitigate these errors, but registration accuracy at sliding interfaces was rarely reported, and global agreement metrics such as segmentation overlap (e.g., a Dice similarity coefficient of 0.95 [23]) do not capture it. Layer-specific local strain values derived by DIR should therefore be regarded as carrying substantial, largely unquantified uncertainty, whereas whole-wall displacement and geometry metrics are likely to be more robust (Table 2).

ARFI, acoustic radiation force impulse; BTA, botulinum toxin A; DRA, diastasis recti abdominis; EO/IO/TrA, external/internal oblique and transversus abdominis; eTEP, enhanced-view totally

extraperitoneal; IH, incisional hernia; IRD, inter-rectus distance; NMES, neuromuscular electrical stimulation; SWE, shear-wave elastography; SWS/SWV, shear-wave speed/velocity; US, ultrasound; VH, ventral hernia. Joppin 2025a and 2025b denote two separate reports.

Discussion

This scoping review identifies a small but rapidly developing literature in which abdominal wall imaging and surface-motion measurement are being repurposed from static anatomical description toward quantitative assessment of mechanical behavior. The inclusion of early pressure-displacement work from 1986 and insufflation-based stress-strain analysis from 2006 also shows that the conceptual foundations of functional abdominal-wall biomechanics predate the recent expansion of elastography and dynamic cross-sectional imaging. The central finding is not that a single modality is ready for clinical adoption, but that multiple technologies are converging on the same conceptual shift (Figure 3): the abdominal wall can be phenotyped by how it deforms, stiffens, contracts, and responds to load, rather than only by defect size and morphology.

Elastography currently has the broadest evidence base and the clearest path to practical accessibility [1–22]. Studies consistently show that measured stiffness depends on disease state, activation state, and acquisition method. This is important because a value obtained during quiet rest cannot be assumed to represent the same construct as one obtained during Valsalva, contraction, or active abdominal inflation. The method is vulnerable to operator-, geometry-, anisotropy-, probe-pressure-, depth-, and layer-related effects [5, 11, 21, 22]. Before any clinical threshold is proposed, acquisition angle, muscle state, probe pressure, ROI, breathing phase, device, and reporting units require standardization and external reproducibility testing. Moreover, because shear-wave speed in the abdominal wall depends on prestress, anisotropy, and layer geometry (Section *Ultrasound elastography and ARFI: stiffness as a candidate imaging biomarker*), shear-wave speed should be reported as the primary output together with the loading state, and derived moduli should not be interpreted as intrinsic, load-independent material constants of the wall.

Dynamic MRI provides the most information-rich whole-wall assessment currently described [23–26]. It can derive spatially resolved deformation, strain, and displacement during physiological tasks. Pressure–motion relationships, however, can be characterized only when intra-abdominal pressure is measured independently and simultaneously, as in the study by Joppin et al. using an ingestible pressure sensor [26], because dynamic MRI alone provides motion but not the load that causes it. Layer-specific strain obtained by registration should also be interpreted in light of the sliding-interface limitations described in Section *Measurement properties and sources of uncertainty*. However, available cohorts are small and post-processing remains demanding. Its most credible current role is therefore as a research platform and potential reference method against which simpler candidate biomarkers can be compared, not as a routine surgical decision tool.

Functional or stress CT occupies an intermediate position because CT is already embedded in complex hernia pathways [27–32]. The reviewed studies provide intuitive outputs such as contractility, stress-induced bulging, defect expansion, displacement, and postoperative contour, but these measures have not been prospectively validated as decision thresholds. Radiation exposure, heterogeneous definitions of 'functional CT', and linked/overlapping cohorts further limit claims of clinical readiness. A crunch acquisition and a Valsalva acquisition represent different loading states and should not be treated as interchangeable.

The newly mapped optical, photogrammetric, and indentation literature adds an important complementary dimension: explicit load-deformation coupling. Pressure-volume compliance, insufflation-derived stress-strain relationships, laser-scanned contraction displacement, full-field DIC strain maps, and indentation coupled to inverse FEA directly address how the abdominal wall responds to known or measurable loading. These approaches are not yet clinically scalable and use different loading environments, but they provide a mechanistic bridge between candidate imaging biomarkers and patient-specific constitutive modeling. They also reinforce marked anisotropy, regional heterogeneity, activation dependence, and inter-individual variability—features that should be considered when simplified scalar stiffness values are interpreted.

What imaging does not yet capture: cyclic and time-dependent behavior

Relating the mapped measurements to the stress–strain relationship (Figure 1) also shows what is missing. In engineering, a load-bearing compound is not designed from single readings but from coefficients and relations obtained under repeated loading, because durability is governed by energy dissipation, permanent deformation, and fatigue rather than by the response to a single load. The abdominal wall and any repair placed in it are loaded cyclically, by breathing, straining, and coughing. Bench models that expose mesh-repaired abdominal wall tissue to repeated, cough-like pressure impacts (dynamic intermittent strain) have shown that repairs can fail under repeated submaximal loads, that failures cluster early in the loading sequence, and that durability depends on the load characteristics and on the mesh–tissue compound as a whole [49, 50]; the same research program has combined such bench-derived relations with rest–Valsalva CT of the individual patient [30–32]. By contrast, the imaging studies mapped here were built around single maneuvers or comparisons between two states. They provide, at best, one or two points on the loading path, often on the strain axis alone, and were not designed to quantify hysteresis, rate dependence, creep, or the change of the response over repeated cycles. Current imaging-derived values therefore cannot yet be translated into the coefficients on which a durable reconstruction would be designed. Closing this gap would require load-referenced, repeated-cycle imaging protocols, for example a standardized series of coughs or Valsalva maneuvers with synchronous intra-abdominal pressure measurement, and direct comparison of the resulting *in vivo* relations with those obtained by cyclic bench testing.

A second major finding is the possible distinction between anatomical severity and mechanical phenotype. Incisional-hernia SWE studies reported associations between disease or

defect width and shear-wave measures [3, 6], while dynamic MRI demonstrated substantial inter-individual variation in motion and pseudo-compliance [25, 26]. These observations support a testable hypothesis that patients with similar static anatomy may differ mechanically; whether such information improves selection of operative strategy or predicts outcomes remains unproven.

Treatment-response imaging is one of the more plausible candidate applications, but it remains early-stage. BTA intentionally alters muscle tone, and functional CT and SWE have detected heterogeneous or longitudinal responses [10, 27, 28]. BTA cleaves SNAP-25 and blocks presynaptic acetylcholine release at the neuromuscular junction, producing a temporary flaccid chemodenervation. Imaging changes observed after BTA (e.g., reduced shear-wave speed/stiffness or altered contractility) may reflect altered neuromuscular activation and the resulting change in resting tone rather than any intrinsic remodeling of the aponeurotic or connective-tissue matrix; with current protocols, post-BTA elastographic and CT changes primarily capture the abolition of active and resting neuromuscular tone, and imaging alone cannot distinguish this neurogenic relaxation from genuine softening or remodeling of the extracellular matrix. The within-patient, own-control design of BTA studies is nonetheless attractive, and separating the two components should be a requirement of future longitudinal protocols, which should incorporate electrophysiological control: concurrent surface or intramuscular EMG to verify and normalize activation level (acknowledging crosstalk and single-point sampling limitations [13, 27]), acquisition at matched activation states (rest with verified electrical silence and a standardized submaximal contraction), and repeat measurements after toxin washout to test whether any change persists once neuromuscular transmission has recovered. The available treated cohorts are small and do not establish thresholds that predict fascial medialization, need for component separation, closure tension, recurrence, or patient-reported recovery. BTA therefore offers a useful experimental model for biomarker validation rather than an already mature imaging-guided pathway.

Postoperative functional imaging is another promising research direction. Dynamic MRI and CT studies demonstrate measurable changes in geometry, displacement, and stress-related contour after reconstruction [25, 29], while ultrasound has been used longitudinally after abdominal-flap surgery and lipoabdominoplasty [18, 33, 34]. These changes are not yet consistently anchored to PROMs, objective trunk performance, return to activity, chronic pain, or recurrence. Without such anchors, it remains uncertain whether an imaging change represents clinically beneficial restoration, compensatory remodeling, or simply a measurable biomechanical difference.

Candidate biomechanical biomarkers in the multifactorial context of hernia repair

Even if validated, imaging-derived mechanical parameters would be only one determinant of surgical strategy and outcome. Recurrence, surgical-site occurrences, bulging, and functional recovery after ventral hernia repair are strongly influenced by patient-related factors (obesity, smoking, diabetes, chronic pulmonary disease, immunosuppression, nutritional status, previous repairs, contamination, loss of domain, and defect size and location) [52, 53] and by biological factors such as altered collagen metabolism, including a reduced type I/III collagen ratio, which may itself contribute to the tissue properties that elastography attempts to capture [66]. Surgeon- and technique-related factors, including experience and case volume, mesh type and position, overlap, fixation, closure technique (e.g., small-bites suture closure), and the use of component separation, are equally important [52, 53, 67]. The relevant question is therefore not merely whether a candidate biomechanical biomarker is associated with an outcome, but whether it adds independent, incremental information beyond established clinical predictors. Future studies should record these variables as covariates, report discrimination and calibration of prediction models with and without candidate imaging biomarkers, and test whether biomarker-informed decisions (e.g., on TAR, BTA timing, or mesh selection) improve outcomes compared with standard care. Biomechanical parameters may prove most useful in patients whose anatomy places them close to existing decision thresholds, such as borderline W2–W3 defects, rather than as stand-alone criteria.

A practical summary for clinicians

To make these possibilities concrete, Table 3 summarizes the candidate clinical applications that recur across the included studies, prediction of primary fascial closure and medialization, monitoring of BTA response, individualized operative planning (e.g., anticipated need for transversus abdominis release or component separation), mesh selection and sizing, prediction of hernia formation or recurrence, and assessment of postoperative function and patient-reported outcomes, together with the candidate biomarker, the current level of evidence, the decision each might inform, and the specific evidence gap that must be closed before clinical use. In every case the current evidence is preliminary and the required next step is prospective validation against the relevant surgical decision or outcome; Table 3 is therefore intended as a research-prioritization aid rather than a menu of ready-to-use tests.

Taken together, the literature supports a reporting framework rather than a treatment algorithm. Every quantitative functional imaging study should specify five linked elements (Figure 4): (1) modality and acquisition parameters; (2) loading or activation maneuver; (3) anatomical structure and ROI; (4) candidate biomarker and unit; and (5) clinical linkage. Reliability, measurement error, and minimal detectable change should be evaluated before cut-offs are proposed. Interventional studies should report absolute values and within-patient change, and candidate biomarkers should be validated against decisions or outcomes meaningful to surgeons and patients. The functional and patient-reported measures catalogued by Brucchi et al. [56] provide natural external anchors.

Proposed research agenda

- Standardize acquisition states, particularly breathing phase, Valsalva instruction, active contraction/crunch technique, patient position, probe pressure, and region-of-interest placement.

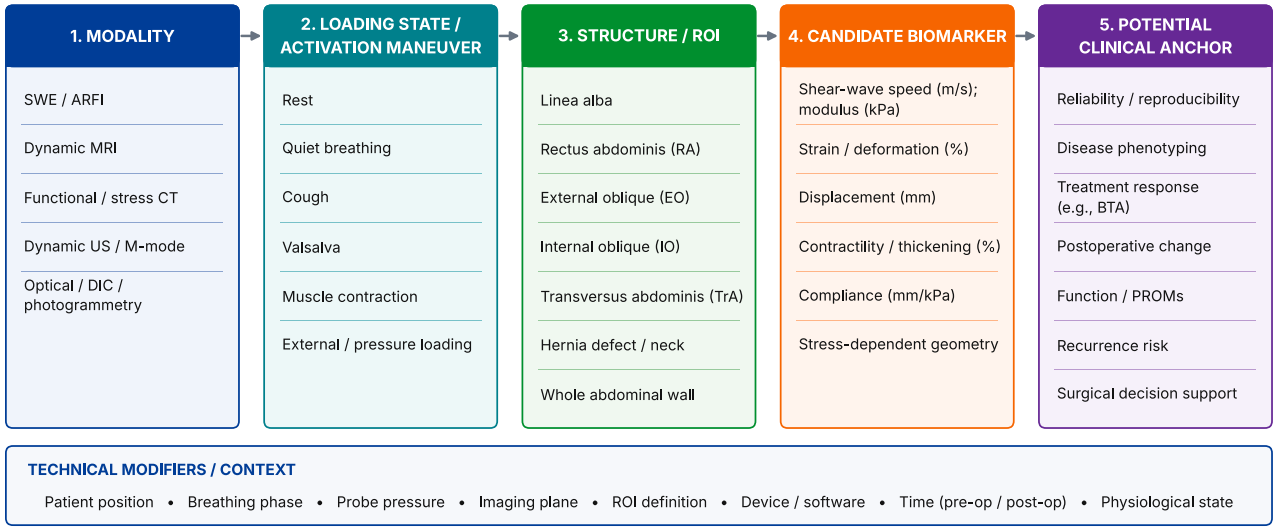


FIGURE 4
Five-element framework for quantitative functional abdominal wall imaging. The proposed framework links five elements that should be reported together: imaging modality; loading state or activation maneuver; anatomical structure or region of interest (ROI); candidate biomechanical biomarker (measured quantity or derived mechanical parameter); and potential clinical linkage. Technical modifiers—including patient position, breathing phase, probe pressure, imaging plane, ROI definition, device/software, timing relative to intervention, and physiological state—may materially influence the measured value. The framework is intended as a reporting and validation structure rather than a clinical decision algorithm. ARFI, acoustic radiation force impulse; BTA, botulinum toxin A; CT, computed tomography; DIC, digital image correlation; MRI, magnetic resonance imaging; PROMs, patient-reported outcome measures; SWE, shear-wave elastography; US, ultrasound.

- Establish modality-specific reproducibility and minimal detectable change before proposing clinical cut-offs.
- Develop normative reference ranges for major muscle groups and the linea alba under clearly defined loading conditions.
- Validate candidate imaging biomarkers against clinically meaningful anchors: fascial medialization, intraoperative closure tension, need for TAR/component separation, PROMs, objective trunk function, return to activity, bulging, and recurrence.
- Prioritize longitudinal within-patient designs before and after BTA and reconstruction, where causal mechanical change is more interpretable than cross-sectional differences.
- Compare lower-cost bedside ultrasound candidate biomarkers with dynamic MRI-derived reference measures to identify clinically scalable surrogates.
- Use external validation and multicenter protocols before integrating imaging-derived biomechanics into treatment algorithms.
- Report shear-wave speed (m/s) as the primary SWE output, together with any derived modulus and its formula, probe orientation relative to fiber direction, and the loading/activation state (and intra-abdominal pressure when measured).
- In BTA studies, incorporate electrophysiological control (EMG), matched-activation acquisition, and post-washout reassessment to separate neurogenic relaxation from tissue change.
- For registration-derived strain, use interface-preserving (sliding-aware) registration and report registration accuracy at fascial interfaces.
- Test the incremental value of candidate biomechanical biomarkers over established patient-, disease-, and surgeon-related predictors in multivariable models.
- Extend imaging protocols from single maneuvers to load-referenced, repeated-cycle acquisitions; report where on the stress–strain relation each measurement lies, together with loading–unloading hysteresis, rate dependence, and cycle-to-cycle change, so that imaging outputs can be related to coefficients derived from cyclic bench testing.

Limitations

This review has several limitations. First, no formal study-level risk-of-bias instrument was applied, consistent with the mapping purpose of the scoping review, although measurement properties and technical limitations were charted descriptively. Second, the evidence base combines healthy mechanistic studies, methodological validation studies, engineering experiments, and clinical cohorts, limiting direct comparison. Third, several cohorts are small, and Kallinowski/GRIP/HEDI reports represent linked or potentially overlapping programs; participant numbers should not be summed across these reports. Fourth, eligibility required judgment at the boundary between diagnostic stress imaging and biomechanical assessment; representative borderline exclusions are therefore reported in Supplementary Table S2. Fifth, Web of Science was added after the initial search, and complete cross-database deduplication was performed retrospectively; although all records were screened against the same criteria and duplicate-pair decisions were concordant except for one record, this sequential process is a deviation from a single prospective deduplication workflow. Sixth, the elastographic and registration-derived values were mapped as reported

by the original authors; they rest on physical and algorithmic assumptions (bulk-wave propagation, isotropy, linear elasticity, smooth displacement fields) that are only partly satisfied in the layered, prestressed abdominal wall, and should not be read as material constants. Seventh, *ex-vivo* tensile testing and cyclic bench testing of repair constructs fell outside the *in vivo* imaging eligibility criteria and were not searched systematically; they are cited as biomechanical context only, and the stress–strain relationship shown in Figure 1 is a schematic that is not derived from the included data. Finally, most studies lack external validation against recurrence, patient-reported function, objective performance, or prospective surgical decision-making.

Conclusion

Quantitative functional imaging of the abdominal wall is an emerging, cross-disciplinary field spanning elastography, dynamic MRI, functional/stress CT, dynamic ultrasound, and optical or surface-mechanics methods. These techniques can measure stiffness, deformation, displacement, contractility, compliance, strain, and stress-dependent geometry *in vivo*, but the evidence remains methodologically heterogeneous and predominantly exploratory. The priority is now standardization of acquisition and measurement properties, followed by prospective validation against outcomes and decisions that matter clinically. Until such validation is available, these candidate biomarkers should be regarded as research measures, interpreted as load- and protocol-dependent quantities rather than intrinsic material constants, rather than established tools for selecting reconstruction strategy, and their ultimate value will depend on the incremental information they add to established patient-, disease-, and surgeon-related predictors. By making the required acquisition, measurement, and clinical-linkage elements explicit (Figures 3, 4; Tables 1–3), this review is intended to serve as a practical framework for designing the standardization and validation studies the field now needs.

Author contributions

FB: Conceptualization, methodology, literature search, data curation, writing – original draft, and writing – review and editing. RS: Methodology, data interpretation, and writing – review and editing. RC: Methodology, supervision, and writing – review and editing. GD: Conceptualization, supervision, and writing – review and editing. All authors contributed to the article and approved the submitted version.

Funding

The author(s) declared that financial support was not received for this work and/or its publication.

Conflict of interest

The author(s) declared that this work was conducted in the absence of any commercial or financial relationships that could be construed as a potential conflict of interest.

Generative AI statement

The author(s) declared that generative AI was used in the creation of this manuscript. During the preparation of this manuscript, the authors used ChatGPT (OpenAI) for language editing, stylistic refinement, and improvement of clarity and readability. Generative AI was not used to generate or analyze study data, determine study eligibility, or make scientific conclusions. All AI-assisted content was critically reviewed and verified by the authors, who take full responsibility for the accuracy, integrity, and final content of the manuscript.

Any alternative text (alt text) provided alongside figures in this article has been generated by Frontiers with the support of artificial intelligence and reasonable efforts have been made to ensure accuracy, including review by the authors wherever possible. If you identify any issues, please contact us.

Publisher's note

All claims expressed in this article are solely those of the authors and do not necessarily represent those of their affiliated organizations, or those of the publisher, the editors and the reviewers. Any product that may be evaluated in this article, or claim that may be made by its manufacturer, is not guaranteed or endorsed by the publisher.

Supplementary material

The Supplementary Material for this article can be found online at: https://www.frontierspartnerships.org/articles/10.3389/jaws.2026.17879/full#supplementary-material

References

1. Tran D, Podwojewski F, Beillas P, Ottenio M, Voirin D, Turquier F, et al. Abdominal wall muscle elasticity and abdomen local stiffness on healthy volunteers during various physiological activities. *J Mech Behav Biomed Mater* (2016) 60:451–9. doi: 10.1016/j.jmbbm.2016.03.001

2. Gabrielsen DA, Carney MJ, Weissler JM, Lanni MA, Hernandez J, Sultan LR, et al. Application of ARFI-SWV in stiffness measurement of the abdominal wall musculature: a pilot feasibility study. *Ultrasound Med Biol* (2018) 44(9):1957–63. doi: 10.1016/j.ultrasmedbio.2018.05.007

3. Wang X, He K, Zhu Y, Fu X, Huang Z, Ding R, et al. Use of shear wave elastography to quantify abdominal wall muscular properties in patients with incisional hernia. *Ultrasound Med Biol* (2020) 46(6):1651–7. doi: 10.1016/j.ultrasmedbio.2020.03.027

4. He K, Zhou X, Zhu Y, Wang B, Fu X, Yao Q, et al. Muscle elasticity is different in individuals with diastasis recti abdominis than healthy volunteers. *Insights Imaging* (2021) 12:87. doi: 10.1186/s13244-021-01021-6

5. Zemzemi C, Catheline S, Turquier F. Shear wave elastography biases in abdominal wall layers characterization. *Phys Med Biol* (2021) 66(20):205006. doi: 10.1088/1361-6560/ac29cd

6. Wang B, He K, Zhu Y, Fu X, Yao Q, Chen H, et al. Quantitative analysis of abdominal muscles using elastography in female patients with incisional hernia. *Front Surg* (2022) 9:831184. doi: 10.3389/fsurg.2022.831184

7. Vergari C, Persohn S, Rohan PY. The effect of breathing on the *in vivo* mechanical characterization of linea alba by ultrasound shearwave elastography. *Comput Biol Med* (2023) 167:107637. doi: 10.1016/j.compbiomed.2023.107637

8. Shehata MA, Khirallah MG, Kurdi M, Abdelwahab SA, Elkhouly R, Gado SE. Mass closure vs. layer-by-layer closure of transverse laparotomy in children: a randomized trial with ultrasound and elastography outcomes. *Front Pediatr* (2025) 13:1655851. doi: 10.3389/fped.2025.1655851

9. Short CL, Morrison T, Crotti TN, Algate K, Gladman MA, Barras CD. An investigation of the functional significance of the pyramidalis muscle using shear wave elastography. *J Anat* (2026) 249:1130–7. doi: 10.1111/joa.70160

10. Rajabzoda RS, Protasov AV, Mazurova OI. Diagnostic value of shear wave elastography in assessing the effectiveness of preoperative botulinum toxin type A therapy in patients with postoperative ventral hernias W3. *Hernia* (2026) 30:315. doi: 10.1007/s10029-026-03812-6

11. MacDonald D, Wan A, McPhee M, Tucker K, Hug F. Reliability of abdominal muscle stiffness measured using elastography during trunk rehabilitation exercises. *Ultrasound Med Biol* (2016) 42(4):1018–25. doi: 10.1016/j.ultrasmedbio.2015.12.002

12. Beamish N, Green N, Nieuwold E, McLean L. Differences in linea alba stiffness and linea alba distortion between women with and without diastasis recti abdominis: the impact of measurement site and task. *J Orthop Sports Phys Ther* (2019) 49(9):656–65. doi: 10.2519/jospt.2019.8543

13. Chino K, Ando R, Suzuki Y. Verification of surface electromyographic activity of the oblique externus abdominis using ultrasound shear wave elastography. *Physiol Rep* (2022) 10(9):e15295. doi: 10.14814/phy2.15295

14. Guo XH, Wang H, Chen SJ, Xie YJ, Liu RR. Multidimensional ultrasound evaluation of diastasis recti abdominis during different gestational periods. *J Ultrasound Med* (2024) 43(3):525–33. doi: 10.1002/jum.16384

15. Kumar ES, Karthiyayini S, Lenin SP, Mithula T. Evaluation of abdominal muscle elasticity and thickness among multiparous women of Indian origin using shear wave elastography and enumerate the factors which influence the parameters: cross-sectional study in a tertiary care hospital. *Res J Med Sci* (2024) 18(1):259–64.

16. Lim Y, Do Y, Lee H. Association between abdominal muscle stiffness, diaphragm thickness and peak expiratory flow in younger *versus* older adults. *Clin Physiol Funct Imaging* (2024) 44(1):63–9. doi: 10.1111/cpf.12850

17. Wang L, Yun T, Zhang D, Zhong J, Yi D, Fu W, et al. A prospective study of two-dimensional ultrasonography combined with shear wave elastography for pregnancy-related diastasis recti abdominis. *Front Physiol* (2024) 15:1382982. doi: 10.3389/fphys.2024.1382982

18. Zhou R, Ding A, Lyu D, Wang C, Wang D. Shear wave elastography for assessment of changes in abdominal soft tissues after lipoabdominoplasty. *Aesthet Plast Surg* (2024) 48:2668–76. doi: 10.1007/s00266-023-03794-1

19. Kozawa K, Nakao G, Nara G, Adachi R, Ishiyama K, Sekiguchi K, et al. Effects of exercise intensity on shear modulus in regional lateral abdominal muscles during the abdominal draw-in maneuver. *J Biomech* (2025) 190:112867. doi: 10.1016/j.jbiomech.2025.112867

20. Bielaczyc G, Simka M. Shear-wave elastography assessment of the linea alba mechanical properties in individuals with obesity *versus* normal-weight: a pilot study. *Int J Abdom Wall Hernia Surg* (2026) 9(1):36–42. doi: 10.4103/ijawhs.ijawhs_125_25

21. Chino K, Kawakami Y, Takahashi H. Tissue elasticity of *in vivo* skeletal muscles measured in the transverse and longitudinal planes using shear wave elastography. *Clin Physiol Funct Imaging* (2017) 37:394–9. doi: 10.1111/cpf.12315

22. Mikołajowski G, Pałac M, Wolny T, Linek P. Lateral abdominal muscles shear modulus and thickness measurements under controlled ultrasound probe compression by external force sensor: a comparison and reliability study. *Sensors* (2021) 21:4036. doi: 10.3390/s21124036

23. Jourdan A, Le Troter A, Daude P, Rapacchi S, Masson C, Bège T, et al. Semiautomatic quantification of abdominal wall muscles deformations based on dynamic MRI image registration. *NMR Biomed* (2021) 34(11):e4470. doi: 10.1002/nbm.4470

24. Jourdan A, Rapacchi S, Guye M, Bendahan D, Masson C, Bège T. Dynamic-MRI quantification of abdominal wall motion and deformation during breathing and muscular contraction. *Comput Methods Programs Biomed* (2022) 217:106667. doi: 10.1016/j.cmpb.2022.106667

25. Joppin V, Bendahan D, El Ahmadi AAE, Masson C, Bege T. Biomechanics of the abdominal wall before and after ventral hernia repair using dynamic MRI. *Hernia* (2025) 29:185. doi: 10.1007/s10029-025-03337-4

26. Joppin V, Jourdan A, Bendahan D, Soucasse A, Guye M, Masson C, et al. Towards a better understanding of abdominal wall biomechanics: *in vivo* relationship between dynamic intra-abdominal pressure and magnetic resonance imaging measurements. *Clin Biomech* (2025) 121:106396. doi: 10.1016/j.clinbiomech.2024.106396

27. Tomazini Martins R, Elstner KE, Skulina C, Rodriguez-Acevedo O, Read JW, Rowe DB, et al. Limitations of electromyography in the assessment of abdominal wall muscle contractility following botulinum toxin A injection. *Front Surg* (2019) 6:16. doi: 10.3389/fsurg.2019.00016

28. Read JW, Ibrahim N, Jacombs ASW, Elstner KE, Saunders J, Rodriguez-Acevedo O. Imaging insights into abdominal wall function. *Front Surg* (2022) 9:799277. doi: 10.3389/fsurg.2022.799277

29. Daes J, Hanssen A, Luque E, Rocha J. Abdominal wall contour and muscle changes after eTEP repair for small ventral hernias and diastasis: a quality improvement study. *Surg Endosc* (2025) 39:4365–75. doi: 10.1007/s00464-025-11816-z

30. Kallinowski F, Ludwig Y, Löffler T, Vollmer M, Lösel PD, Voß S, et al. Biomechanics applied to incisional hernia repair – considering the critical and the gained resistance towards impacts related to pressure. *Clin Biomech* (2021) 82:105253. doi: 10.1016/j.clinbiomech.2020.105253

31. Kallinowski F, Gutjahr D, Harder F, Sabagh M, Ludwig Y, Lozanovski VJ, et al. The grip concept of incisional hernia repair—dynamic bench test, CT abdomen with valsalva and 1-Year clinical results. *Front Surg* (2021) 8:602181. doi: 10.3389/fsurg.2021.602181

32. Lösel PD, Relle JJ, Voß S, Raschidi R, Nessel R, Görich J, et al. Clinical application of HEDI for biomechanical evaluation and visualisation in incisional hernia repair. *Commun Med (Lond)* (2026) 6:68. doi: 10.1038/s43856-025-01311-w

33. Seidenstuecker K, Legler U, Munder B, Andree C, Mahajan A, Witzel C. Myosonographic study of abdominal wall dynamics to assess donor site morbidity after microsurgical breast reconstruction with a DIEAP or ms-2 TRAM flap. *J Plast Reconstr Aesthet Surg* (2016) 69(5):598–603. doi: 10.1016/j.bjps.2015.11.007

34. Lee SJ, Lim J, Tan WTL, Baliarsing A, Iau PTC, Tan LKS, et al. Changes in the local morphology of the rectus abdominis muscle following the DIEP flap: an ultrasonographic study. *Br J Plast Surg* (2004) 57:398–405. doi: 10.1016/j.bjps.2003.12.014

35. Biały M, Adamczyk W, Gnat R, Stranc T. Tissue deformation index as a reliable measure of lateral abdominal muscle activation on M-mode sonography. *J Ultrasound Med* (2017) 36(7):1461–7. doi: 10.7863/ultra.16.07045

36. Biały M, Adamczyk WM, Stranc T, Szlachta G, Gnat R. M-mode ultrasound evaluation of lateral abdominal muscle postural response to load: an exploratory study. *J Ultrason* (2024) 24:37. doi: 10.15557/JoU.2024.0037

37. Brown SHM, McGill SM. An ultrasound investigation into the morphology of the human abdominal wall uncovers complex deformation patterns during contraction. *Eur J Appl Physiol* (2008) 104:1021–30. doi: 10.1007/s00421-008-0858-8

38. Vasseljen O, Fladmark AM, Westad C, Torp HG. Onset in abdominal muscles recorded simultaneously by ultrasound imaging and intramuscular electromyography. *J Electromyogr Kinesiol* (2009) 19:e23–e31. doi: 10.1016/j.jelekin.2007.07.013

39. Goldman JM, Rose LS, Morgan MDL, Denison DM. Measurement of abdominal wall compliance in normal subjects and tetraplegic patients. *Thorax* (1986) 41:513–8. doi: 10.1136/thx.41.7.513

40. Song C, Alijani A, Frank T, Hanna GB, Cuschieri A. Mechanical properties of the human abdominal wall measured *in vivo* during insufflation for laparoscopic surgery. *Surg Endosc* (2006) 20:987–90. doi: 10.1007/s00464-005-0676-6

41. Lubowiecka I, Szepietowska K, Tomaszewska A, Bielski PM, Chmielewski M, Lichodziejewska-Niemierko M, et al. A novel *in vivo* approach to assess strains of the human abdominal wall under known intraabdominal pressure. *J Mech Behav Biomed Mater* (2022) 125:104902. doi: 10.1016/j.jmbbm.2021.104902

42. Becker C, Plymale MA, Wennergren J, Totten C, Stigall K, Roth JS. Compliance of the abdominal wall during laparoscopic insufflation. *Surg Endosc* (2017) 31:1947–53. doi: 10.1007/s00464-016-5201-6

43. Todros S, de Cesare N, Pianigiani S, Concheri G, Savio G, Natali AN, et al. 3D surface imaging of abdominal wall muscular contraction. *Comput Methods Programs Biomed* (2019) 175:103–9. doi: 10.1016/j.cmpb.2019.04.013

44. Remus R, Sure C, Selkmann S, Uttich E, Bender B. Soft tissue material properties based on human abdominal *in vivo* macro-indenter measurements. *Front Bioeng Biotechnol* (2024) 12:1384062. doi: 10.3389/fbioe.2024.1384062

45. Troka M, Szepietowska K, Lubowiecka I. Self-organising maps in the analysis of strains of human abdominal wall to identify areas of similar mechanical behaviour. *J Mech Behav Biomed Mater* (2024) 156:106578. doi: 10.1016/j.jmbbm.2024.106578

46. Fung YC. *Biomechanics: Mechanical Properties of Living Tissues*. 2nd ed. New York: Springer (1993).

47. Deeken CR, Lake SP. Mechanical properties of the abdominal wall and biomaterials utilized for hernia repair. *J Mech Behav Biomed Mater* (2017) 74:411–27. doi: 10.1016/j.jmbbm.2017.05.008

48. Holzapfel GA. *Nonlinear Solid Mechanics: A Continuum Approach for Engineering*. Chichester: Wiley (2000).

49. Kallinowski F, Baumann E, Harder F, Siassi M, Mahn A, Vollmer M, et al. Dynamic intermittent strain can rapidly impair ventral hernia repair. *J Biomech* (2015) 48(15): 4026–36. doi: 10.1016/j.jbiomech.2015.09.045

50. Lesch C, Ludwig Y, Kugel F, Uhr K, Vollmer M, Nessel R, et al. Cyclic pulse loads pave the road to the GRIP concept in abdominal wall reconstruction. *Mini-invasive Surg* (2023) 7:25. doi: 10.20517/2574-1225.2023.31

51. FDA-NIH Biomarker Working Group. *BEST (Biomarkers, Endpoints, and Other Tools) Resource. Silver Spring (MD): Food and Drug Administration (US)*. Bethesda (MD): National Institutes of Health US (2016). Available online at: https://www.ncbi.nlm.nih.gov/books/NBK326791/ (Accessed September 2026).

52. Liang MK, Holihan JL, Itani K, Alawadi ZM, Gonzalez JRF, Askenasy EP, et al. Ventral hernia management: expert consensus guided by systematic review. *Ann Surg* (2017) 265(1):80–9. doi: 10.1097/SLA.0000000000001701

53. Sanders DL, Pawlak MM, Simons MP, Aufenacker T, Balla A, Berger C, et al. Midline incisional hernia guidelines: the european hernia society. *Br J Surg* (2023) 110(12): 1732–68. doi: 10.1093/bjs/znad284

54. Jairam AP, Timmermans L, Eker HH, Pierik REGJM, van Klaveren D, Steyerberg EW, et al. Prevention of incisional hernia with prophylactic onlay and sublay mesh reinforcement *versus* primary suture only in midline laparotomies (PRIMA): 2-year follow-up of a multicentre, double-blind, randomised controlled trial. *Lancet* (2017) 390(10094):567–76. doi: 10.1016/s0140-6736(17)31332-6

55. HerniaSurge Group. International guidelines for groin hernia management. *Hernia* (2018) 22(1):1–165. doi: 10.1007/s10029-017-1668-x

56. Brucchi F, Gilardini R, Vetere A, Sassun R, Robecchi Majnardi A, Muysoms F, et al. Abdominal wall function in hernia and diastasis: systematic review of evaluation methods and clinical relevance. *Hernia* (2026) 30(1):79. doi: 10.1007/s10029-025-03557-8

57. Arksey H, O'Malley L. Scoping studies: towards a methodological framework. *Int J Soc Res Methodol* (2005) 8(1):19–32. doi: 10.1080/1364557032000119616

58. Levac D, Colquhoun H, O'Brien KK. Scoping studies: advancing the methodology. *Implement Sci* (2010) 5:69. doi: 10.1186/1748-5908-5-69

59. Peters MDJ, Marnie C, Tricco AC, Pollock D, Munn Z, Alexander L, et al. Updated methodological guidance for the conduct of scoping reviews. *JBI Evid Synth* (2020) 18(10):2119–26. doi: 10.11124/JBIES-20-00167

60. Tricco AC, Lillie E, Zarin W, O'Brien KK, Colquhoun H, Levac D, et al. PRISMA extension for scoping reviews (PRISMA-ScR): checklist and explanation. *Ann Intern Med* (2018) 169(7):467–73. doi: 10.7326/M18-0850

61. Munn Z, Peters MDJ, Stern C, Tufanaru C, McArthur A, Aromataris E. Systematic review or scoping review? Guidance for authors when choosing between a systematic or scoping review approach. *BMC Med Res Methodol* (2018) 18:143. doi: 10.1186/s12874-018-0611-x

62. Gennisson JL, Deffieux T, Macé E, Montaldo G, Fink M, Tanter M. Viscoelastic and anisotropic mechanical properties of *in vivo* muscle tissue assessed by supersonic shear imaging. *Ultrasound Med Biol* (2010) 36(5):789–801. doi: 10.1016/j.ultrasmedbio.2010.02.013

63. Brum J, Bernal M, Gennisson JL, Tanter M. *In vivo* evaluation of the elastic anisotropy of the human achilles tendon using shear wave dispersion analysis. *Phys Med Biol* (2014) 59(3):505–23. doi: 10.1088/0031-9155/59/3/505

64. Gennisson JL, Rénier M, Catheline S, Barrière C, Bercoff J, Tanter M, et al. Acoustoelasticity in soft solids: assessment of the nonlinear shear modulus with the acoustic radiation force. *J Acoust Soc Am* (2007) 122(6):3211–9. doi: 10.1121/1.2793605

65. Schmidt-Richberg A, Werner R, Handels H, Ehrhardt J. Estimation of slipping organ motion by registration with direction-dependent regularization. *Med Image Anal* (2012) 16(1):150–9. doi: 10.1016/j.media.2011.06.007

66. Henriksen NA, Yadete DH, Sorensen LT, Ågren MS, Jorgensen LN. Connective tissue alteration in abdominal wall hernia. *Br J Surg* (2011) 98(2):210–9. doi: 10.1002/bjs.7339

67. Deerenberg EB, Harlaar JJ, Steyerberg EW, Lont HE, van Doorn HC, Heisterkamp J, et al. Small bites *versus* large bites for closure of abdominal midline incisions (STITCH): a double-blind, multicentre, randomised controlled trial. *Lancet* (2015) 386(10000): 1254–60. doi: 10.1016/S0140-6736(15)60459-7

10.3389/jaws.2026.17879

Glossary

Stress (σ) Force per unit cross-sectional area of a material (N/m^2 = Pa; usually kPa or MPa for soft tissue). For the intact wall, the corresponding structural quantities are intra-abdominal pressure and membrane tension (force per unit width, N/mm).

Reference configuration The state of the tissue from which deformation is measured. *Ex vivo* it is the unloaded, stress-free specimen; *in vivo* it is, in this review, the resting abdomen, which is already prestressed.

Cauchy (true) stress Force per unit of current (deformed) area. It is the stress actually acting in the tissue and the measure meant by "stress" throughout this review.

Piola–Kirchhoff stresses Stress measures referred to the reference configuration. The first (nominal or engineering stress) is force per unit of reference area; the second is defined entirely in the reference configuration and is paired with the Green–Lagrange strain in hyperelastic models. They equal Cauchy stress only at small deformation.

Strain (ε) Change in length relative to the original length (dimensionless, often given in %). Circumferential, radial, and principal strains describe its direction; Green–Lagrange strain is a definition suited to large deformations.

Stress–strain curve The curve relating stress to strain for a material loaded in a defined direction (Figure 1). Its structural counterparts are the force–displacement and pressure–volume curves of the whole wall. It is the basic relation to which every measurement in this review is referred.

Toe region The initial, low-slope part of the stress–strain curve of collagenous tissue, in which wavy (crimped) fibers straighten and re-orient, so that large strain is produced by little stress.

Linear region The steeper, approximately straight part of the curve that follows the toe region and the transitional heel, in which the recruited fibers themselves bear load.

Stiffness Resistance to deformation, i.e., the slope of a load–deformation curve. Material stiffness is a modulus (kPa); structural stiffness is force per unit displacement (N/mm) and depends on geometry and thickness as well as on the material.

Young's modulus, E Slope of the stress–strain curve in tension. It is a single constant only for linear materials; for soft tissue it varies along the curve.

Tangent modulus The local slope of a nonlinear stress–strain curve at a given operating point. Small-perturbation methods such as elastography return a tangent stiffness.

Shear modulus, μ Resistance to a shape change at constant volume (kPa). In shear-wave elastography it is derived from shear-wave speed as $\mu = \rho c^2$; for an isotropic, incompressible material $E \approx 3\mu$.

Shear-wave speed, c Speed (m/s) at which a small transverse wave travels through tissue; the quantity actually measured by SWE and ARFI.

Compliance The inverse of stiffness: deformation obtained per unit load (e.g., volume or displacement change per unit pressure).

Prestress Stress already present in the tissue before the measurement, here imposed by intra-abdominal pressure and muscle tone. It determines the operating point on the stress–strain curve.

Strain stiffening Nonlinearity of soft tissue: the reversible increase of stiffness with increasing strain along the J-shaped curve; the reason why a stiffness value is meaningful only together with the load at which it was obtained.

Anisotropy Dependence of mechanical properties on direction, here caused by the orientation of muscle and collagen fibers.

Viscoelasticity Time-dependent behavior: the response depends on loading rate; the tissue elongates slowly under constant load (creep) and its stress decays under constant deformation (stress relaxation).

Hysteresis Difference between the loading and unloading paths of the stress–strain curve; the enclosed area is the energy dissipated in one cycle.

Cyclic loading Repeated application of load, as in breathing or coughing. In soft tissue the first cycles differ from later ones until a repeatable response is reached (preconditioning).

Fatigue; low-cycle fatigue Progressive damage and failure under repeated loads below the single-load strength. Low-cycle fatigue denotes failure after relatively few cycles at loads high enough to cause permanent deformation in each cycle.

Strain hardening In materials science, the increased resistance to further deformation that follows permanent (plastic) deformation. It is cycle- and time-dependent and should not be confused with reversible strain stiffening.

Constitutive model A mathematical description of the stress–strain behavior of a material; hyperelastic models (e.g., Ogden) describe large, nonlinear elastic deformation. Inverse finite-element analysis estimates their parameters by fitting a computer model to measured loads and deformations.

Acoustoelastic effect Dependence of wave speed on the stress in the tissue; it makes shear-wave speed rise with wall tension.

Guided (Lamb) waves Waves confined by the boundaries of a thin layer; their speed depends on layer thickness and frequency and does not equal the bulk shear-wave speed.

DIR and DIC Deformable image registration and digital image correlation: computational methods that estimate displacement fields by matching image content between two acquisitions (DIR, volumetric images) or surface patterns between photographs (DIC); strain is obtained as the spatial derivative of displacement.

Biomarker (three levels) Measured quantity, mechanical parameter, and biomarker are the three levels distinguished in this review (Introduction): what the device records; a coefficient or relation derived from it through a stated model; and a quantity of either kind that has been shown, under a defined loading state, to carry reliable clinical information.